Phase Separation and Persistent Magnetoresistive Memory Effect in $La_{0.375}Pr_{0.25}Ca_{0.375}MnO_3$ Thin Films

研 究 生 ：蔡於璁

指導教授 ： 莊振益教授

Table of Contents

Abstract

Phase separation (PS) theory has drawn intensive attention in explaining the colossal magnetoresistance (CMR) effects nowadays. However, although displaying the same CMR phenomena as $La_{1-x}Ca_xMnO_3$(LCMO), $(La_{1-x-y}Pr_x)Ca_yMnO_3$ (LPCMO) shows another tremendous characteristics: a hysteresis in cooling and subsequent warming in both temperature-dependent resistance (R(T)) and magnetization (M(T))! In this thesis, aware of the more glassy-separated phase existences in LPCMO, we presume this hysteresis resulting from the long time relaxation behavior. As a consequence, we conducted a detailed study on the persistent magnetoresistive memory effect (PMME), which is believed to be intimately related to the detailed process toward to equilibrium state of a glassy phase coexistent system. The quality of the LCMO and LPCMO samples was carefully characterized by measuring the R(T) and M(T). The crystalline structure and electronic structure of the films were checked by x-ray diffraction (XRD) and x-ray absorption near edge (XANE) spectroscopy. In particular, LPCMO thin film, showing CMR effect, was taken to conduct temperature-dependent PPME experiments.

From the results, we obtained the equilibrium states of resistance of LPCMO at various temperatures, proposed a picture within a phase-size-related PS regime, and explained this glassy phase coexist system different with the not-glassy phase coexist system in LCMO.

Chap.1 Introduction

Though the first report of manganites was published in 1950 [1], it was not until about

a decade ago that manganites started to draw tremendous attention from both the

academic and industrial areas. The main reason that revives these extensive research

interests on manganites is largely due to the "colossal" magnetoresistance (CMR)—a

MR ratio over 10^6 % obtained in mid-1990s. [2]. Zener first proposed his seminal

double-exchange (DE) model to describe the simultaneous abrupt changes in the

temperature-dependent behaviors in electric transport and magnetic properties that were

later coined as CMR [3]. However, as pointed out by Millis *et al.* [4], the DE model

alone was not enough to give a quantities account on the experimentally observed CMR

effect. By considering the crystal structure and the influence of Coulombic interaction of

CMR materials, the Jahn Teller effect was introduced and probed [4-7]. More recently

besides the DE model and the incorporation of Jahn-Teller effect developed in early days,

nowadays the phase separation (PS) scenarios have been put forth as alternatives in

explaining CMR effects. [8-15]

In this study, we tried to unveil the influence of PS nature on the electric transport of

$La_{0.375}Pr_{0.25}Ca_{0.375}MnO_3$ (LPCMO) thin film, one of well-characterized CMR materials

[16-22]. In this material the time-relaxation behavior of resistance at various applied

fields may reflect a significant phenomenon associated with the competition between

charge ordering (CO) and ferromagnetic-metal (FM) phases especially near the transitions. It denotes that the resistance continuously changes upon time after the disturbing factors ceased to acting may have been the process approaching the equilibrium distribution of coexisting phases. [23-26] This behavior observed in LPCMO is apparently a strong support to the PS model, especially when we are looking for the equilibrium state at various temperatures. The importance of the equilibrium state cannot be over emphasized since the equilibrium state is the ground base of theoretical models aimed to interpreting the exotic yet frequently variable transport behaviors exhibited in the family of CMR manganites. Nevertheless, measurement of the actual equilibrium resistance of LPCMO is a difficult, if not impossible, job in lab, since the relaxation time is usually way too long for realistic to laboratory experiments. As a consequence, albeit over fifty years since CMR materials were discovered, only few indirect experiment data showed the probable equilibrium state of temperature-dependent resistance (R(T)) in LPCMO by measuring the persistent magnetoresistive memory effect, in a narrow temperature region. Undoubtedly, the discussion or study limited in that region is not adequate to lend a complete interpretation of transport characteristics of LPCMO. In this study we conducted systematic measurement of persist magnetoresistive memory effect (PMME) at various temperatures and applied fields. We then establish equilibrium state of the resistance of LPCMO over a wide range of temperatures and compared that with

the phase separation evolution process as depicted in Fig. 1[14]. We focus on the y=0.25

Pr doping concentration which has been demonstrated to have phases evolution from two

short range (s-r) phases to final two long range phases with decreasing temperatures.

Furthermore, the evolution of phases was evidently supported from the observation of

the resistance response to applied magnetic filed oscillation.
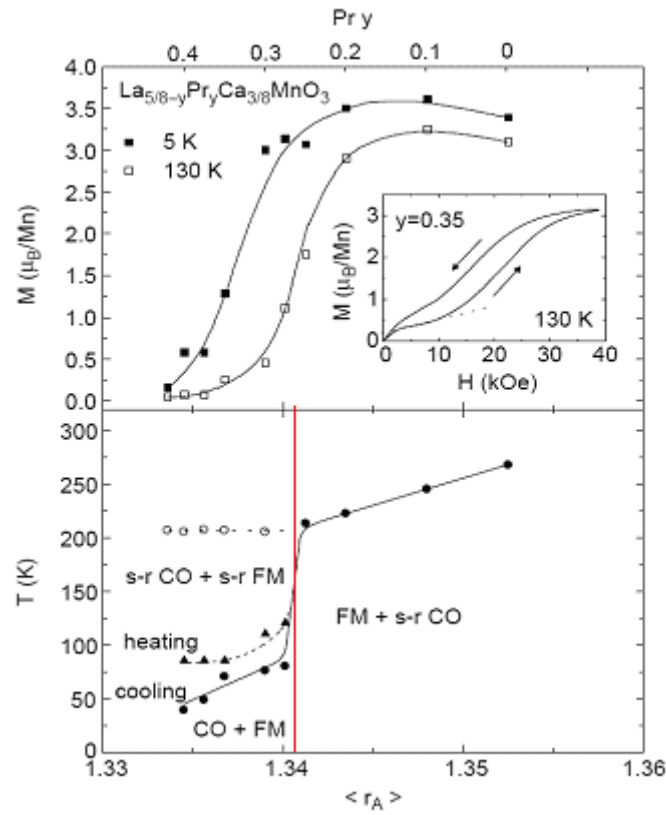
Fig.1 $<r_A>$ donates the average ionic size. "y" is doping concentration of Pr. The lower

plot reveals different phase-coexistence at various temperatures. The red line is the guide

of the eye for y=0.25. [14]

Chap. 2 Fundamental Phenomenologies of CMR materials

a. Phenomenology of CMR Materials

Magneto-resistance (MR) refers to the resistance changes of material in response to the applied magnetic fields. The MR ratio is defined as follows:

$$MR \ \ ratio = \frac{R_H - R_0}{R_0} \quad , \qquad (1)$$

where R_H is the resistance measured under an applied magnetic field and R_0 is the resistance obtained at zero field. The MR phenomenon has been the subject for a great deal of recent research interest, because of the improvement and invention of commercially available technologies – magnetic sensors, magnetic recording heads and magnetic memories, to name a few. There have been many kinds of MRs (AMR, TMR, GMR) studied and applied for years, each with distinctly different transport mechanisms. The colossal magneto-resistance (CMR) we discuss in this study is named because the MR exhibited is "colossal" as compared to other MR effects. For example, the MR ratio of "giant" magneto-resistance (GMR) is approximately 10~30%, while the MR ratio of certain manganites can be about 1500%! As an example, in Fig. 2, we show the typical CMR behaviors as a function of the applied field for our LPCMO films.
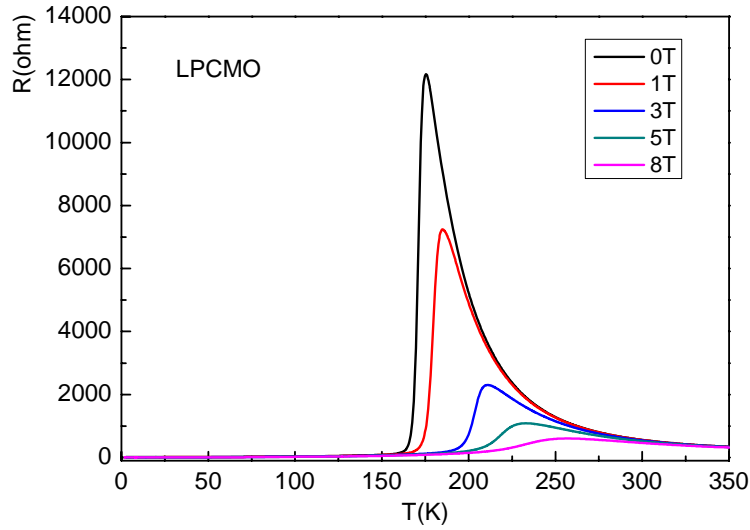
Fig.2 The resistance-temperature dependence at various magnetic applied field of

LPCMO thin film is displayed. The plot shows a huge MR ratio (98%) at 175k.

b. The Double-Exchange Model

To explain the simultaneous occurrence of arising ferromagnetism and insulating to

metallic transport behaviors in manganites, an indirect coupling, between the electrons

residing at the incomplete d-shells of Mn is realized, via conduction electrons by

hopping around Mn-O-Mn configurations. Since the coupling is indirect, the electron

hopping must occur twice from Mn through O, to another Mn, it was termed as a

"double-exchange" mechanism as illustrated schematically in Fig.3. Zener stated that for

each Mn ion, the incomplete d-shells must be occupied by electrons in accordance to the

Hund's rule, which means that unpaired spins in d-shells of each Mn ion are all aligned

to maximize the magnetic moment [3]. It is conceived that if the net spins of the

incomplete *d*-shells are all aligned parallel, i.e. in the ferromagnetic state, conduction

electrons would be able to lower their kinetic energy and conduct electricity more easily

due to the minimization of spin scattering.
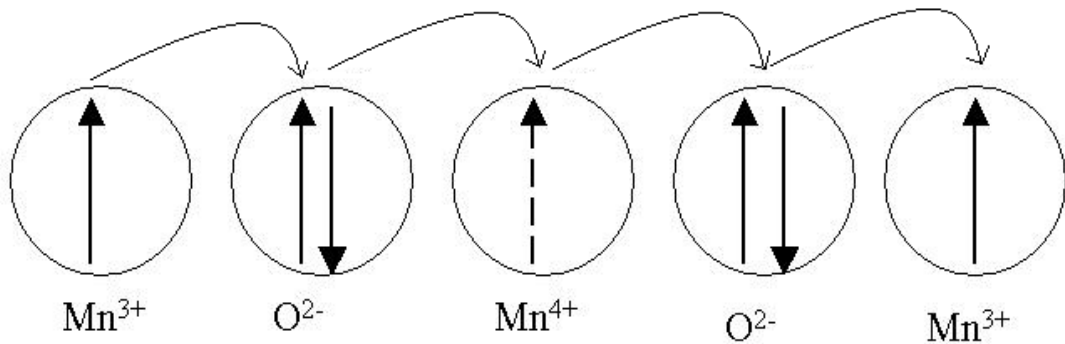
Fig.2 The conduction electron's "double exchange" is displayed here twice, suggesting

the process of electric transport along with the magnetic spin alignment.

c. Perovskite Structures & the Jahn Teller effect

However, the DE model failed to interpret the CMR phenomena in a quantitative

manner [27]. The polaron mechanism along with phonons or magnons was proposed in

trying to account for the discrepancies left by the DE model [5-7,28]. The crystal

structure of manganites is belong to a lattice system generally called as perovskite

structure [29](Fig.4). Apparently, since the electron hopping process only involves Mn

and O ions, if we exclude other ions, an MnO_6 octahedral cage emerges. Now let's recall

the electronic configuration of *d*-shells shown in Fig.5. Corresponding to six O ions

around Mn ion, we can see that the degeneracy of Mn *d*-level will be lifted and broken

into two groups, one identified as e_g band consisting of $d_{x^2-y^2}, d_{3z^2-r^2}$ and the other

identified as t_{2g} band consisting of d_{xy}, d_{yz}, d_{xz} orbitals. It will be clearer if we take a look

at the shapes of these orbitals. The overlapped area of $d_{x^2-y^2}, d_{3z^2-r^2}$ with O ion is larger

than that between d_{xy}, d_{yz}, d_{xz} and O ion. The Columb repulsion naturally explains the

broken degeneracy and that the e_g band is at the higher energy level. This is also referred

to as the crystal field effect [30]. Moreover, the degeneracy of the two orbitals in the e_g

band can be further lifted because of the Jahn-Teller distortion (JTD)[4,7], namely the

stretch along z-axis of MnO_6, as depicted in Fig.6. The occurrence of JTD is driven by

the additional lowering of the ground state energy. With the JTD, the $d_{3z^2-r^2}$ state will

overlap less area with O ion, leading to a lower-energy ground state. Similarly, the

$d_{x^2-y^2}$ will be forced to a higher energy level as a result of the increasing overlapped-area.
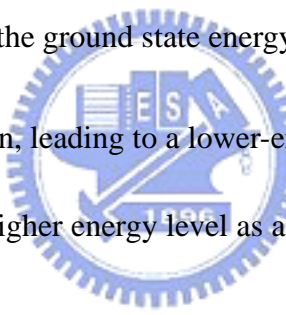
It is worth noting that JTD only happened in the situation of MnO_6 octehedra with

Mn^{3+} as JTD only affects the electron on e_g state where there are four electrons in

d-shells. MnO_6 octehedra with Mn^{2+} will not distort, attributed to the five electrons fully

occupying spin-up states. As to MnO_6 octehedra with Mn^{4+}, the JTD won't lower the

energy because there is no electron in the e_g band.
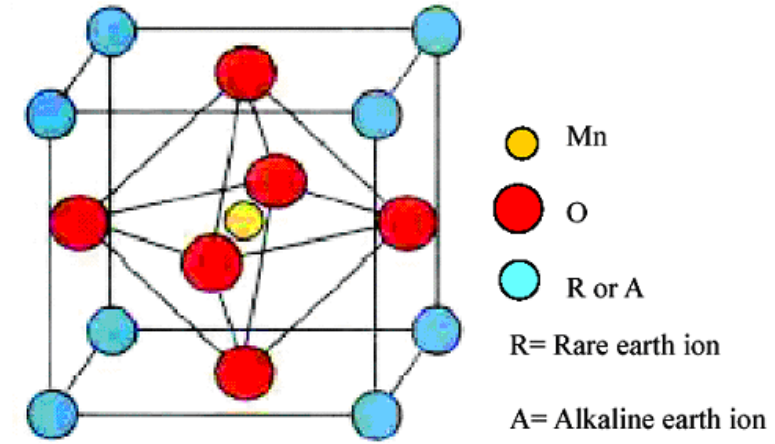
Fig.4 The diagram of perovskite structure displays the position of each ions.
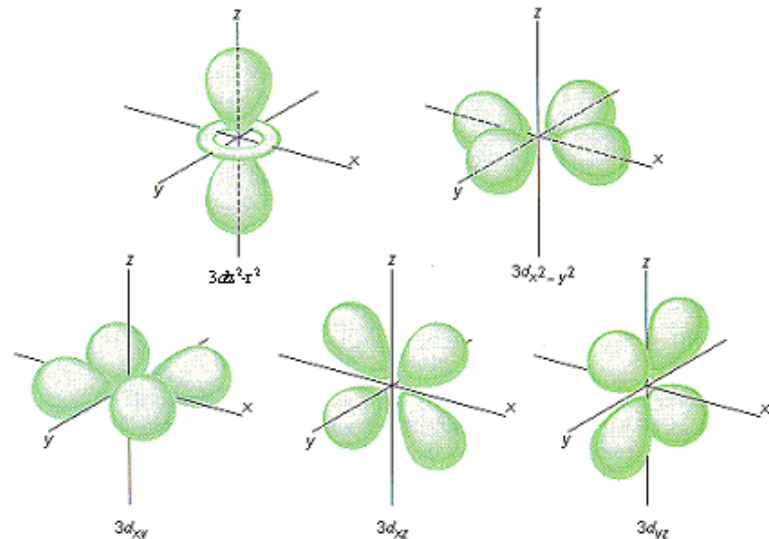
Fig.5 The electronic configuration of *d*-shells of Mn includes $3d_{x^2-y^2}$ and $3d_{x^2-y^2}$

belonging to e_g band, and $3d_{xy}$, $3d_{xz}$ and $3d_{yz}$ belonging to t_{2g} band. The crystal field

is responsible for these two splitting bands as a result of different orbital symmetries.
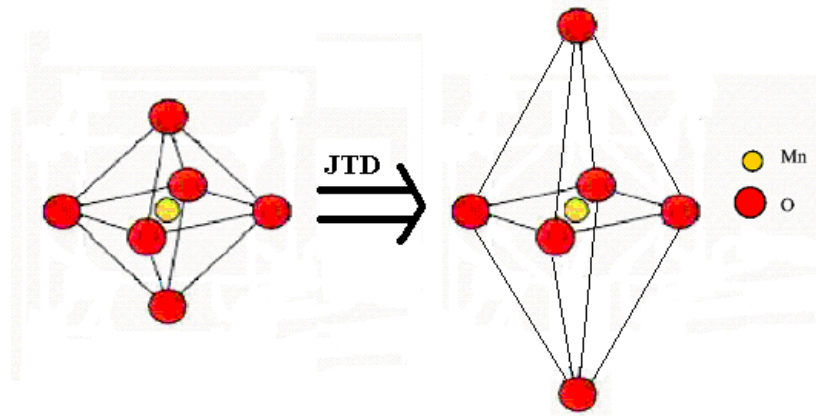
Fig.6 Jahn-Teller distortion stretches the z-axis of MnO_6, lowering the energy of ground state.

d. Phase Separation (PS)

Phase separation (PS), a manifestation of electronic inhomogeneities in manganites, has drawn increasing attention from researchers recently [31-33]. In this scenario, two distinct phases with different magnetical and electronic structures coexist and compete with each other. It is this competing behavior that dominates the electronic and magnetic transport. Theoretical calculations considering PS have been carried out, for example, for one-orbital model [32]. Moreover, many experiment results suggested that the inhomogeneities in manganites system in various length scales, such as nanometer clusters and micrometer ones. As an example, Fig. 7 shows the scanning tunneling microscopy (STM) works displaying regions with different conductivities for $La_{0.7}Ca_{0.3}MnO_3$ films in ferromagnetic-metallic state [34].
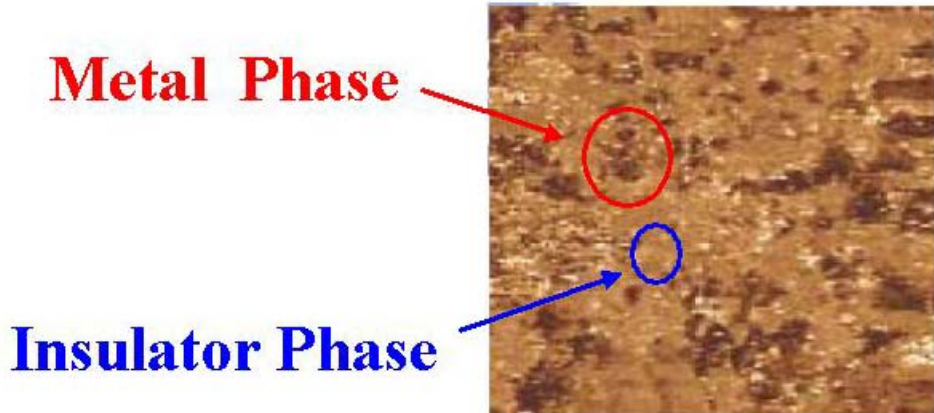
Fig.7 The phase separation of $La_{0.7}Ca_{0.3}MnO_3$ thin film at T=88 K is observed from STM work. [34]

e. Percolation

To account for the electric transport behavior within the context of PS model the

percolation mechanism was developed with PS model. The main idea of percolation

is "sufficient links." First of all, we regard the amounts of insulating and conducting

"phases" as two different links in a two-dimension square, shown schematically in Fig.8.

The amount of conducting phase grows as the temperature decreases. As a consequence,

the conducting paths, reach to a critical portion of the square, forming a metallic

conducting path for electrons to transport. This is how percolation theory demonstrates

the sudden drop of resistivity at the emergence of sudden increase of magnetization due

to the ferromagnetic transition at the Curie temperature T_c [32].
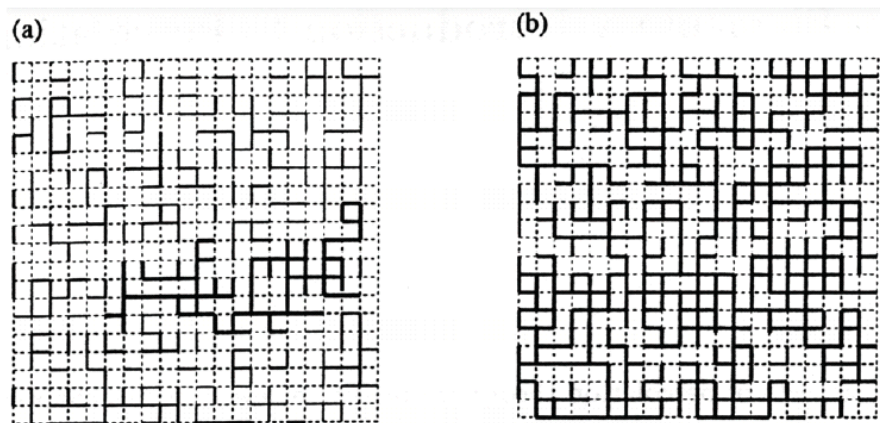
Fig.8 f: the fraction of metal phase. Dark and thicker lines represent the metal links. (a)f=0.4,insulating(b)f=0.7,conducting.[35]

Chap. 3 Experiments

a. Sample Preparation

(a)Target Fabrication
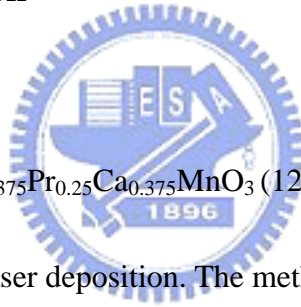
We synthesized the $La_{0.375}Pr_{0.25}Ca_{0.375}MnO_3$ (12g) and $La_{0.625}Ca_{0.375}MnO_3$ (12g) targets

for the need of the pulse laser deposition. The method we applied is a standard solid-state

route. Take $La_{0.375}Pr_{0.25}Ca_{0.375}MnO_3$ target for example, starting from preheated $MnCO_3$,

Pr_6O_{11}, $CaCO_3$, and La_2O_3 powders, we mixed them together with proportions of aimed

stoichiometry -$MnCO_3$(6.720g), Pr_6O_{11}(2.487g), $CaCO_3$(2.194g), and La_2O_3(3.571g)-

and heated this mixture to promote reactions among the constituents at 1200℃ for 8

hours; the solidified mixture was then grinded and pressed using a mold to form the

target body; the target body was heated again at 1250℃ for 12 hours. This final

procedure was repeated three times with an incremental heating temperature of 50℃

each time. The final sintering process was conducted at 1400℃ and furnace cooled over

several hours to room temperature. $La_{0.625}Ca_{0.375}MnO_3$ target was fabricateded by the same method, as well.

(b) Pulse Laser Deposition (PLD)

Briefly, the basic concept of pulse laser deposition (PLD) is to apply pulsed intense photons accompanied with large energy to ablate the materials form the target and deposit it onto the chosen substrate. In practice, a successful PLD fabrication requires correct conditions, which includes the deposition temperature, the output power of the excimer laser beam, the pressure of O_2, and the choice of substrates. As to our samples, $La_{0.375}Pr_{0.25}Ca_{0.375}MnO_3$ and $La_{0.625}Ca_{0.375}MnO_3$ thin films, the PLD fabrication procedures are as following: first we chose $NdGaO_3$ as our substrates for its lattice constant (3.86 anstrom) being closest to our materials (3.87 anstrom) as compared to that of $LaAlO_3$ and $SrTiO_3$ (Table 1). The scheme of the PLD set-up is shown in Fig.9 with a base pressure of 2×10^{-5} torr. We precisely tuned the O_2 pressure to 0.3 torr by needle valve and controlled the deposition temperature at 700℃ with the heater behind the holder and the thermal couple imbedded in the holder on which the $NdGaO_3$ substrate was attached. The 248 nm KrF excimer laser pulses with 350 mJ and repetition rate 3 Hz was then guided into the chamber by UV mirrors and lens, as depicted in Fig.9. Afterward, the film was cooled in 400 torr O_2 environment to room temperature with the heater off. The typical thickness of both $La_{0.375}Pr_{0.25}Ca_{0.375}MnO_3$ and $La_{0.625}Ca_{0.375}MnO_3$

films was about 250 nm with the LCMO being deposited at a slightly higher deposition

temperature 720℃.

	NdGaO$_3$	LaAlO$_3$	SrTiO$_3$
Lattice mismatch	~0.3%	~1.6%	~0.5%

Table 1. Comparison of several substrates by lattice mismatch with LCMO/LPCMO

lattice constant 3.87 anstrom.
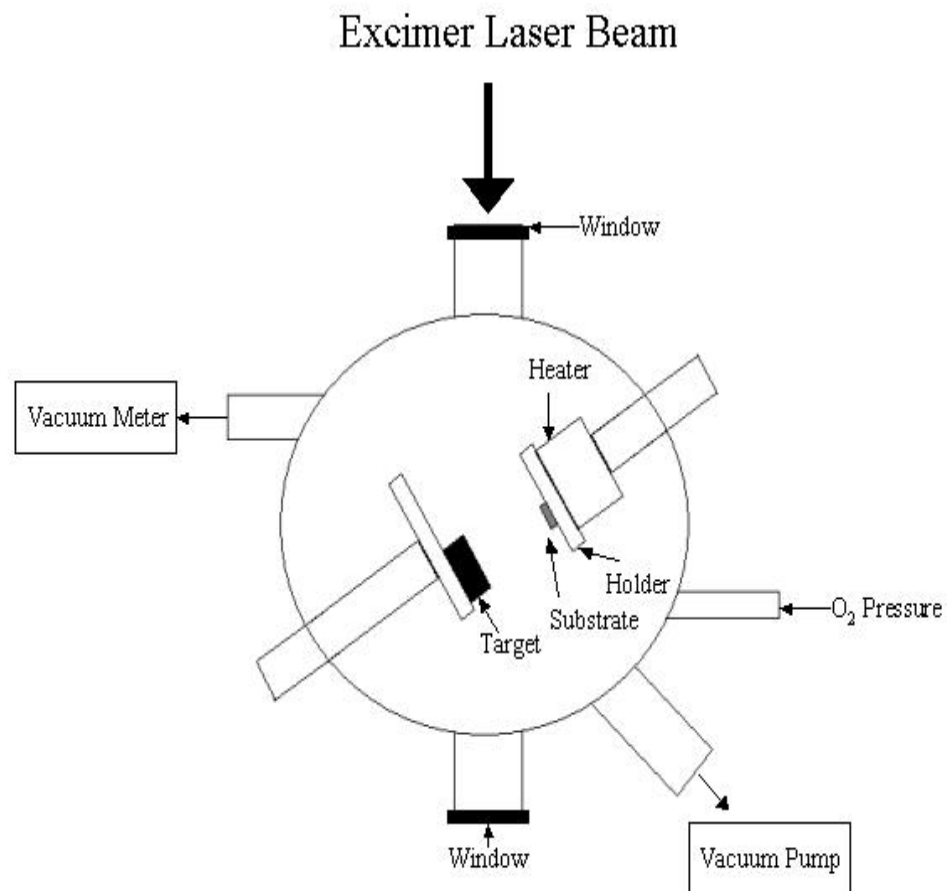
Fig.9 The configuration of PLD system

b. Characterization of Thin Film

(a) X-ray Diffraction (XRD)

X-ray diffraction (XRD) measurement has been a useful tool to check the crystal structure of samples. Based on Bragg diffraction condition:

$$n\lambda = 2d \sin \theta \qquad (2)$$

where n is an integer, λ is the wavelength of the x-ray, d is the distance between successive parallel planes, and θ is the angle between incident x-ray and the normal line of the lattice plane.
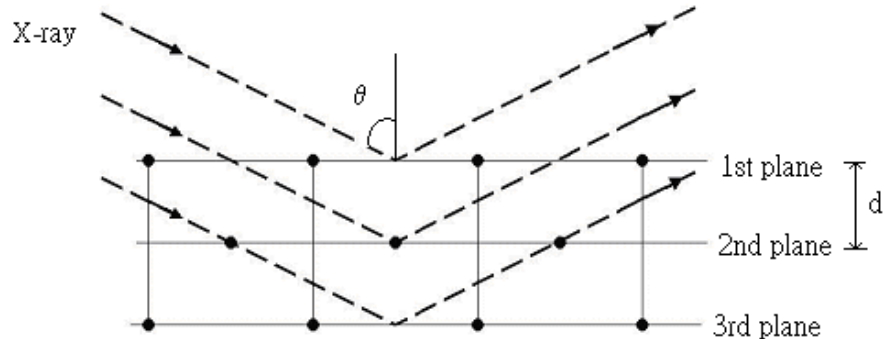
Fig. 10 The illustration of XRD process. θ denotes the angle between incident x-ray and the normal line of lattice planes.

In addition, the pattern of XRD also has to meet the requirement of the structure factors and atomic form factors. X-ray patterns of our samples are displayed in Fig.11, along with the pattern of the $NdGaO_3$ substrate for comparison. Obviously we can assure our thin films were well crystallized with preferred c-axis oriented growth. In separate

measurements of films grown with similar conditions it has been demonstrated that

these PLD manganite films retained excellent epitaxial relations with the substrate..
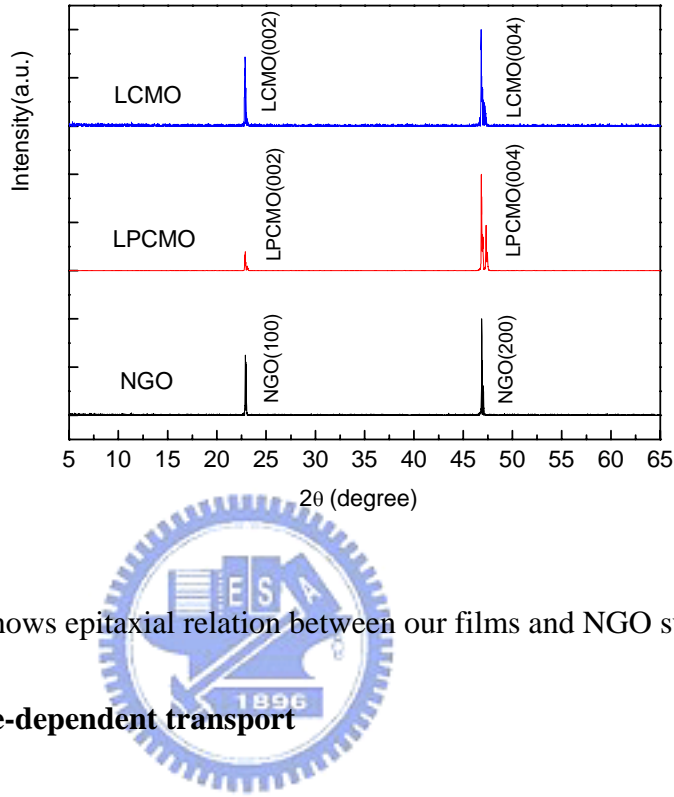
Fig.11 XRD shows epitaxial relation between our films and NGO substrates.

(b) Temperature-dependent transport

The standard four-probe configuration is employed to measure the resistance of

samples. The traditional two-probe configuration (Fig.12) could leave us all the

resistances (R_M) from contact pads (R_P), from lines (R_L), and from the sample (R_S):

$$R_M = \frac{V_{AB}}{I} = \frac{(I-i)\times(R_S + 2R_L + 2R_P)}{I}$$
$$\because i \approx 0 \Rightarrow I - i \approx I \Rightarrow R_M = R_S + 2R_L + 2R_P$$

(3)
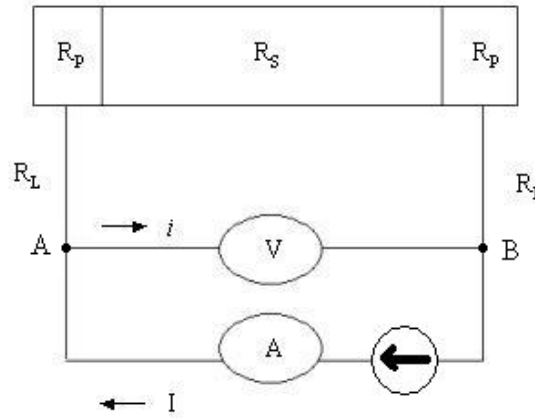
Fig. 12 The configuration of two-probe resistance measurement system.

By separating current-source pads and voltage- meter pads, we can avoid the combined voltage-drop including pad resistance, line resistance and the sample resistance and measure the exact resistance of the sample. This method is generally referred as standard four-probe measurement (Fig.13). In this configuration:

$$R_M = \frac{V_{AB}}{I} = \frac{(I-i) \times R_S + i \times (2R_L + 2R_P)}{I}$$

$$\because i \approx 0 \Rightarrow I - i \approx I \Rightarrow R_M = \frac{I \times R_S + 0}{I} = R_S$$

(4)
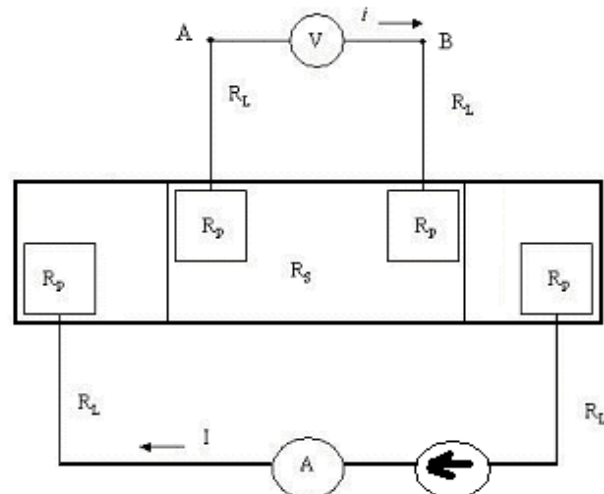
Fig. 13 The configuration of four-probe resistance measurement system.

The resistance-temperature dependences of LCMO and LPCMO thin films are displayed in Fig.14 and Fig.15. As shown in both samples, the resistance increases with decreasing temperature, indicative of an insulating behavior. Nevertheless, when the temperature reaches T_p, a sudden drop of resistance occurs at T_p, and the resistance kept decreasing with the lowering temperature, revealing a typical metallic behavior. Particularly, along with the process of cooling and subsequent warming, we observed the hysteresis phenomenon in LPCMO thin film.
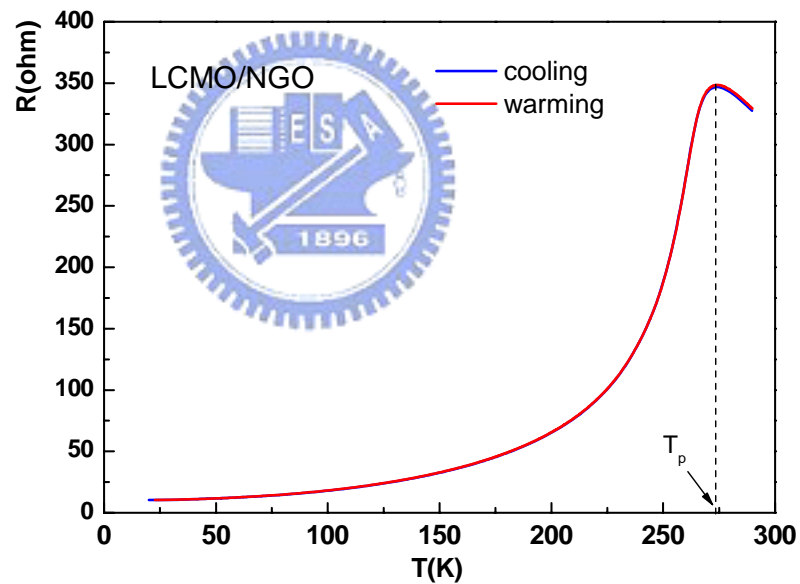
Fig.14 The resistance-temperature dependence of LCMO is plotted with T_p at 270 K.
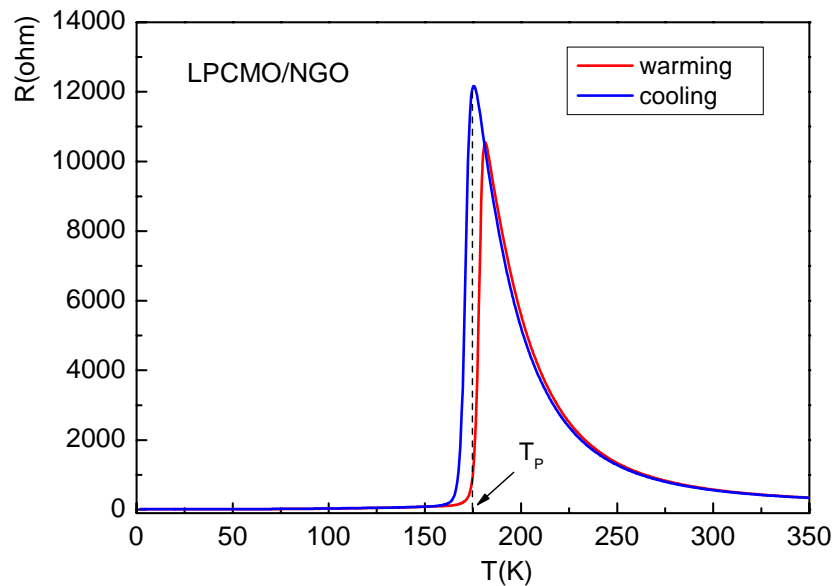
Fig.15 The resistance-temperature dependence of LPCMO is plotted with T_p at 175K.

The plot shows the clear hysteresis of LPCMO.

(c) Magnetization-Temperature Dependence

The temperature-dependent magnetization (M(T)) was measured using the Quantum

Design Superconducting Quantum Interference Device (SQUID) system. Fig. 16 shows

the M(T) result of LCMO, displaying a paramagnetic to ferromagnetic transition around

T= 270K. On the other hand, Fig. 17 shows the M(T) of LPCMO film. It is evident that,

similar to that observed in R(T), the M(T) of LPCMO also displays a clear hysteresis.
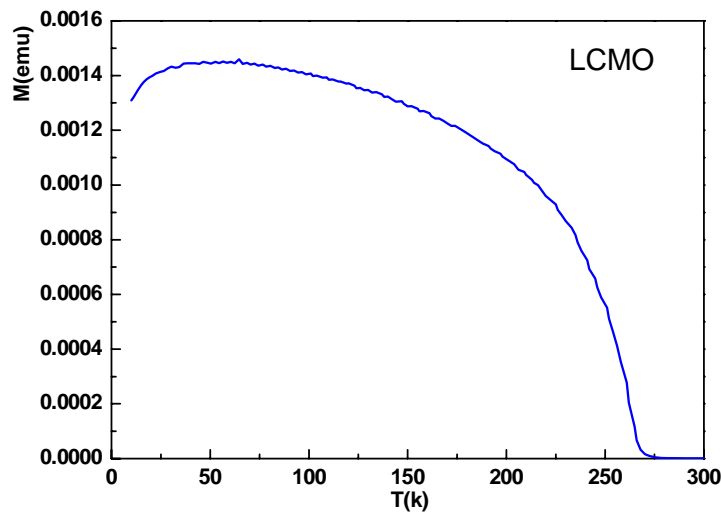
Fig.16 The magnetization-temperature (MT) dependence of LCMO is shown. The

saturation of magnetization at low temperature indicates the FM.
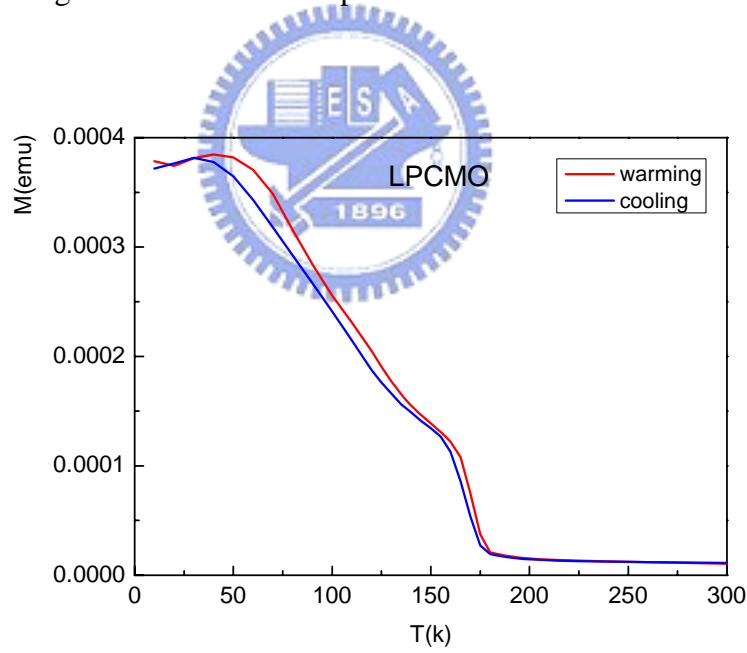

Fig.17 The temperature-dependent magnetization (MT) of LPCMO. Notice that in

addition to the saturation of magnetization exhibited at low temperature, a significant

hysteresis in M(T) is evident over a wide range of temperatures.

(d) X-ray Absorption Near Edge Spectroscopy (XANES)

The dramatic variations in electrical and magneto properties accompanied with the paramagnetic-ferromagnetic transition at T_c and insulator-metal transition at T_p is believed to be intimately associated with the electronic structure change of the perovskite manganites. In order to detect the electronic structures, the x-ray absorption spectroscopy (XAS) has become a rather important tool [39-45]. Fig. 18 illustrates the various processes involved when an energetic photon is absorbed by the atoms. Essentially, the incident x-ray with the energy in the order of several hundred eV allowed the core level electrons of a particular atom of interest (A) to promote to the higher level (B) followed by dipole selection rule with no spin changes. As the excited electron relaxed back to the core level, the electron occupying at level B absorbed the energy from the relaxation and produced fluorescence photon, most of which further excited the Auger electron. Therefore, we can obtain the spectrum from both fluorescence photon and Auger electrons and delineate the relevant electronic structure change due, for example, to environmental change of the particular ions.
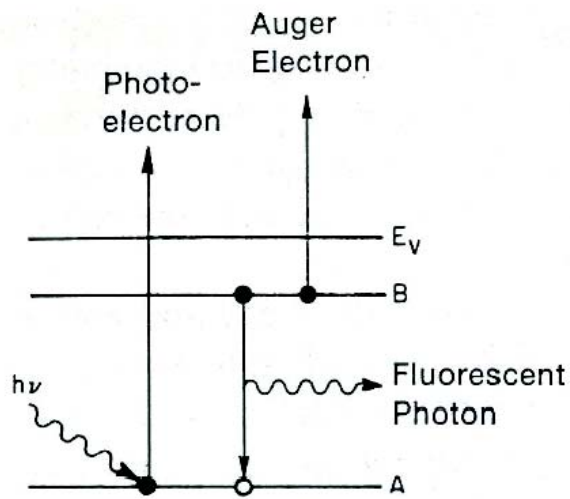
Fig.18 The diagram shows the process of XAS. The incident x-ray excited the core

electron and after the relaxation of the excited electron, the fluorescent photon and the

Auger electron could be detected.
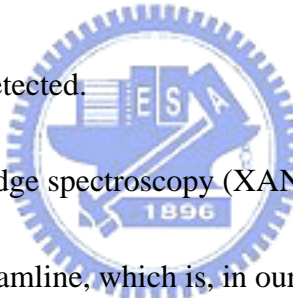
X-ray absorption near-edge spectroscopy (XANES) requires the high-energy spherical

grating monochromater beamline, which is, in our case, at the National Synchrotron

Radiation Research Center, Taiwan, to permit x-ray absorption for XANES. The base

pressure in the spectrometer chamber was better than 10^{-9} torr; the resolution of the

spectra was 0.22eV controlled by the spherical grating monochromater; and the standard

procedure to remove the background contribution and to normalize the intensity was

adopted. Hereby, we first checked the Mn L-edge XANES of our samples as a

fingerprint to assure the Mn ions consisting of both Mn^{3+} and Mn^{4+}(Fig. 19). Comparing

with the shape of the standard samples, Mn_2O_3 and MnO_2, we can approximately regard

Mn ions of our samples as the combination of Mn^{3+} and Mn^{4+}. Also, because the splitting

behavior occurring at low temperature at the pre-edge of O K-edge was intensely

discussed by researchers, the O K-edge XANES of LCMO and LPCMO were displayed

for comparison. As is evident from Fig. 20, the absorption peak of the O K-edge XANES

shows the peak-splitting behavior at low temperature (LT) for the LCMO sample

(Fig.20). While for LPCMO sample such LT peak-splitting behavior is absent (Fig. 21).

Among the models describing this splitting behavior, our results appear to support the

picture chematically depicted in Fig. 22. In this picture, it is conceived that the JTD

induces significant change in the electronic structure. At room temperature (RT), the

larger JTD leads to the strong hybridization of the $d_{x^2-y^2}$ state of $e_g(\uparrow)$ band with the t_{2g}

$(\downarrow)$ states; at low temperature (LT), the diminishing JTD leads to a much weaker

hybridization and thus the $d_{x^2-y^2}$ state of $e_g(\uparrow)$ band is further separated from the t_{2g}

$(\downarrow)$ states and is manifested as the peak splitting. It is possible that due to the smaller

exchange interaction energy, the hybridization in LPCMO is so strong that the difference

of JTD at RT and at LT could not be distinguished.

Mn-$L_{2,3}$ XANES spectra at T = 300 K
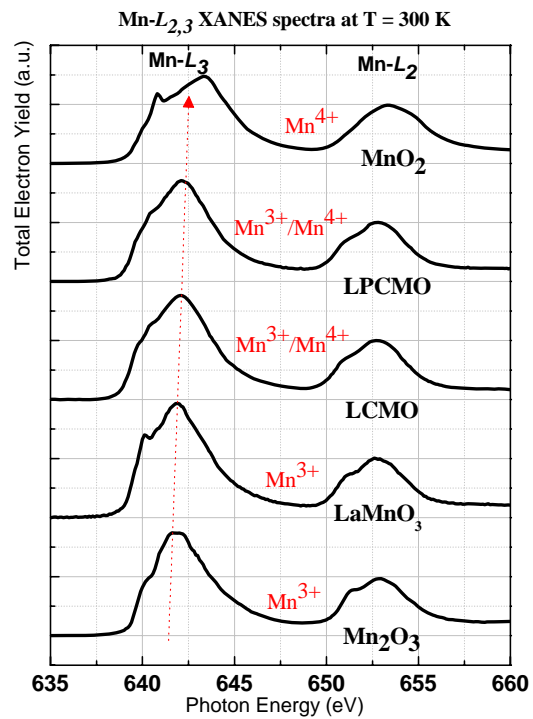
Fig. 19 The Mn L-edge XANES of LCMO and LPCMO displays the shape in

similarity of the combination of the shape of MnO_2 and Mn_2O_3.
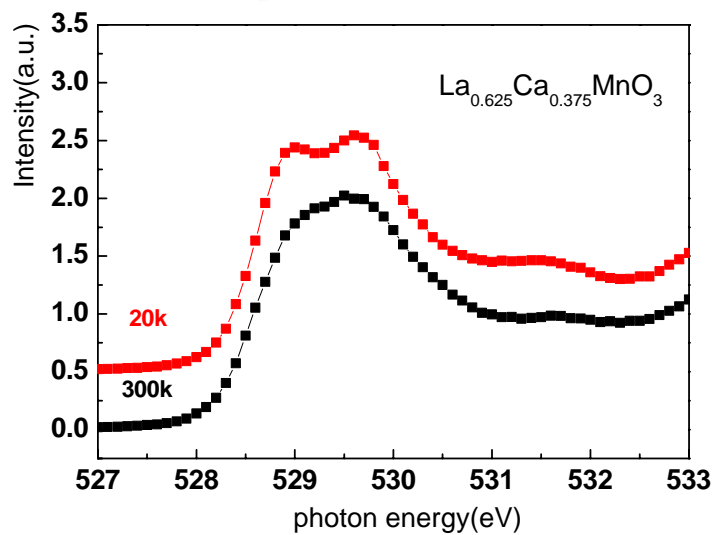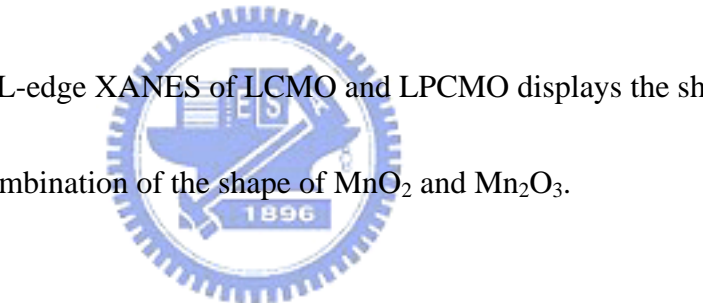
Fig. 20 The temperature-dependent XANES of LCMO is displayed. We can observe

the splitting behavior at 529.5 eV at T = 20 K, comparing to the peak at T = 300 K.
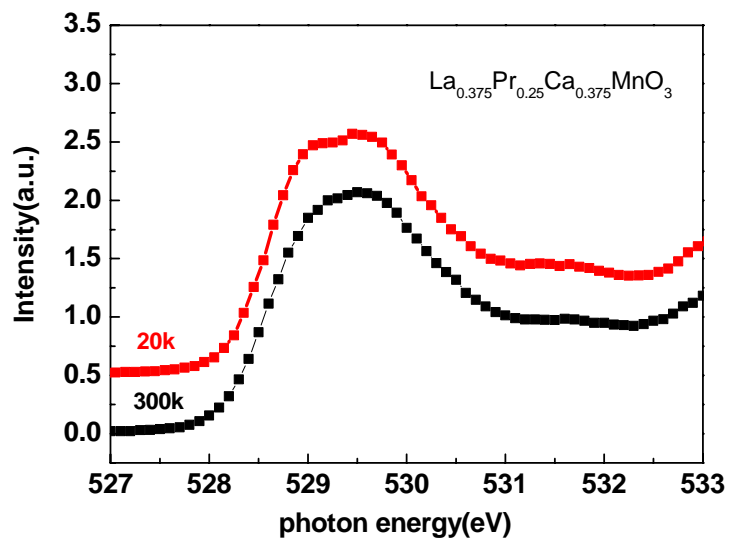
Fig.21 The temperature-dependent XANES of LPCMO reveals the disappearance of

the splitting behavior at T = 20 K.
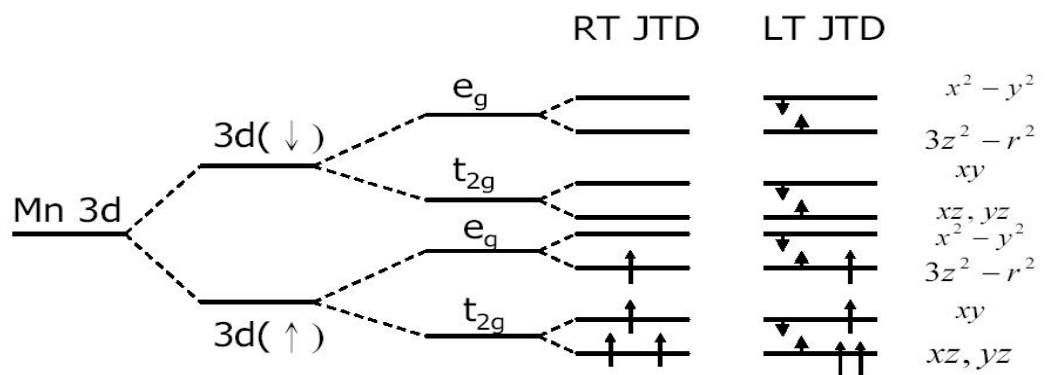
Fig.22 The schematic diagram displays the process of breaking the degeneracy of Mn

3d states. In this model, the $d_{x^2-y^2}$ state of $e_g(\uparrow)$ states closely hybridized with the t_{2g} ($\downarrow$)

states. The small arrows indicate the suppression of JTD at LT.

c. Time-relaxation Behavior Measurement

—The Persistent Magnetoresistive Memory Effect (PMME)

The resistance of LPCMO sample would relax with the elapsed time to the

equilibrium state below charge-ordering temperature. However, no matter the resistance

increased or decreased upon time, the relaxation time period for laboratory experiments

is too long. Due to the obstacle of waiting the sample to approach the equilibrium state,

we adopted the method originally used by P. Levy et al. to perform experiments on this

persistent magnetoresistive memory effect (PMME). [25]; This method is done as

following. Under a cooling protocol to a certain temperature we applied a magnetic field

to disturb the distribution of the coexisting phases; here it is to enhance the growth of the

metallic phase. Then after removing the applied field, we measured the tendency of the

resistance relaxation. Fig. 23 illustrates the procedures of this experiment. The resistance

would not rejuvenate to its virgin value, if there exists the PMME. Furthermore,

depending on the magnitudes of applied field, two following situations could happen.

Either the resistance decreased or increased as a function of time. A threshold field H_{th} is

then determined. By definition, after we applying field above H_{th}, the ulterior relaxation

of the resistance reversed its sign. Several models have been proposed to explain this

phenomenon. One of the purposes of this study is to clarify the dominant mechanism

leading to this phenomenon.
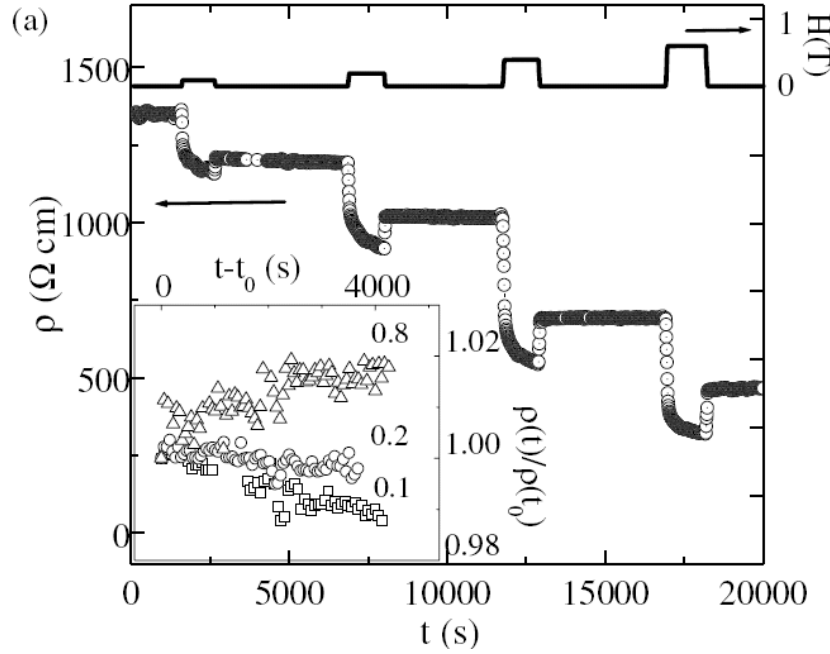
Fig. 23 The upper part of this diagram shows the appliance and removal of **H** with

time evolution. The resistance changes upon this time period were measured. The inset

indicates the reverse sign of the tendency.

In addition, this method could also help us find the equilibrium state of sample

resistance at various temperatures because it must be lying somewhere between the

minimum of the decreasing resistance and the maximum of the increasing one. Before

we get into the detailed discussion of the PMME results, we first show the experimental

results of LCMO and LPCMO respectively in Fig. 24 and Fig. 25. It is evident that

complete rejuvenation of resistance in obtained for LCMO, indicating an absence of

PMME for this material. On the contrary, for LPCMO, the also relaxation towards the

equilibrium resistance is observed after the removal of the applied field. The behavior

also is very much dependent on the strength of the applied field. Although it is not clear

at present the actual mechanism, giving rise to the difference between LCMO and

LPCMO, it is, nevertheless, quite consistent with the hysteretic behavior of the R(T) and

M(T) results described above. We suspect that, although both materials are found to have

phase coexistent over wide range of temperatures, the formation of the coexistent phases

may have very different natures. Namely, we note that in LCMO the coexisting phases

are the parent paramagnetic insulating phase and newly formed ferromagnetic metallic

phase. While for LPCMO, the phases transition involves a pair of new phases (the CO

and FM phases) are formed from a single paramagnetic phases when temperature is

lowered below T_{CO} In any case, since the PMME is only observable in LPCMO, we will

focus on discussion of this effect on this particular material.
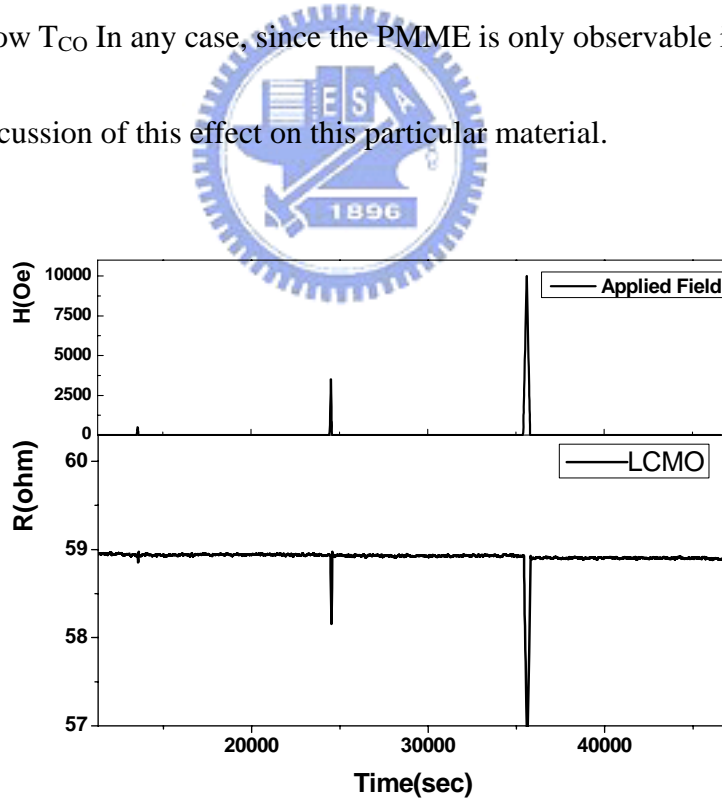
Fig. 24 The resistance remained almost the same after removals of different applied

magnetic field impulses.
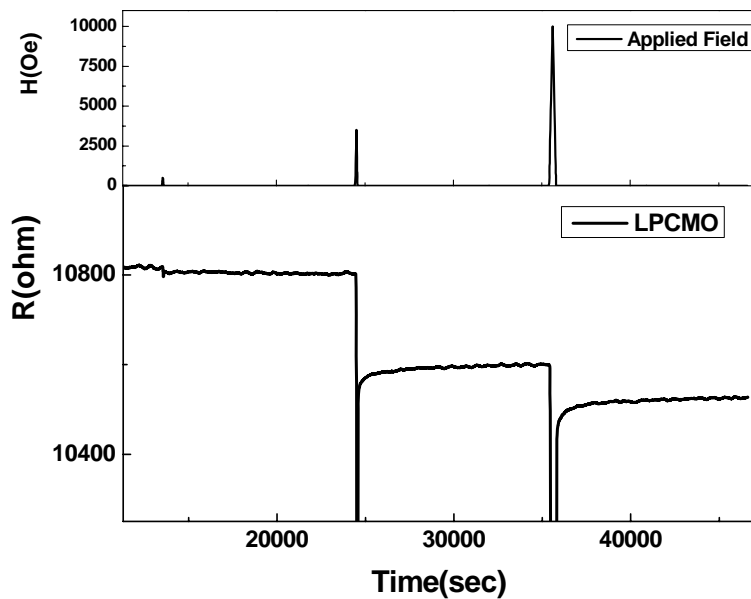
Fig.25 The drop of the resistance did not rejuvenate to its original value after removal

of the applied magnetic field impulses.

Chap. 4 Results and Discussions

a. Persistent Magnetoresistive Memory Effect (PMME) on LPCMO thin film

(a)Anisotropy of Persistent Mangetoresistive Memory Effect (PMME)

In order to delineate the intrinsic characteristic of the epitaxial thin films, whether the

anisotropy of applied magnetic field existed deserved to be confirmed. The experiment

procedure is as following: we first cooled the sample to T= 174 K, the middle point of

the R(T) hysteresis in zero applied field, at a constant rate of 3 K/ min; next, after

waiting for 90 minutes for the resistance to relax, a small magnetic field of 200Oe was

applied for another 90 minutes; then the magnetic field was removed and completed as

one 180-minute cycle. Same cycles were repeated with larger and larger magnetic field

up to 1 Tesla. Fig. 26(a) shows the results for in-plane applied field. Notice that below a

field denoted as H_{th} the relaxation is descending while above that an ascending relaxation

is evident. (See the circles shown in Fig. 26(a) and the enlarged version shown in Fig.

26(b).) For fields applied perpendicular to the film surface, similar behaviors were

observed, except that H_{th} in this case is much larger (~1T) as compared to the in-plane

field (H_{th}~0.1T).
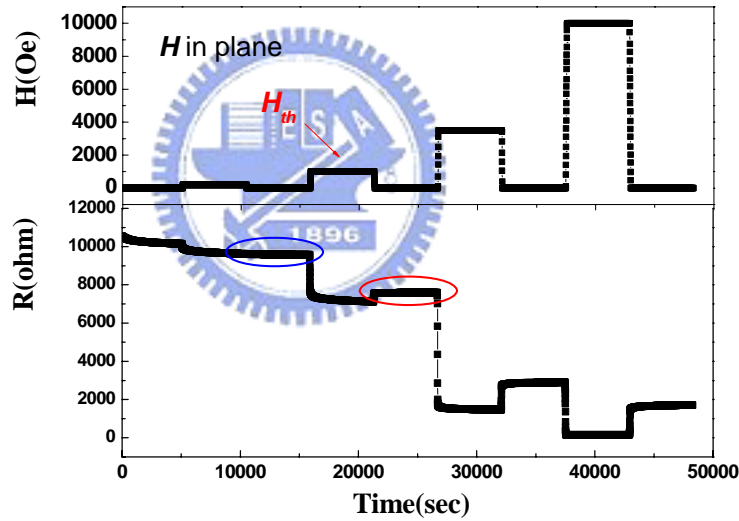
Fig.26 (a) The process of **H**-in-plane experiment with time evolution is illustrated. The

drop of the resistance caused by magnetic field represents normal MR effect. We marked

H_{th} as a threshold magnetic field that reversed the resistance relaxation tendency.
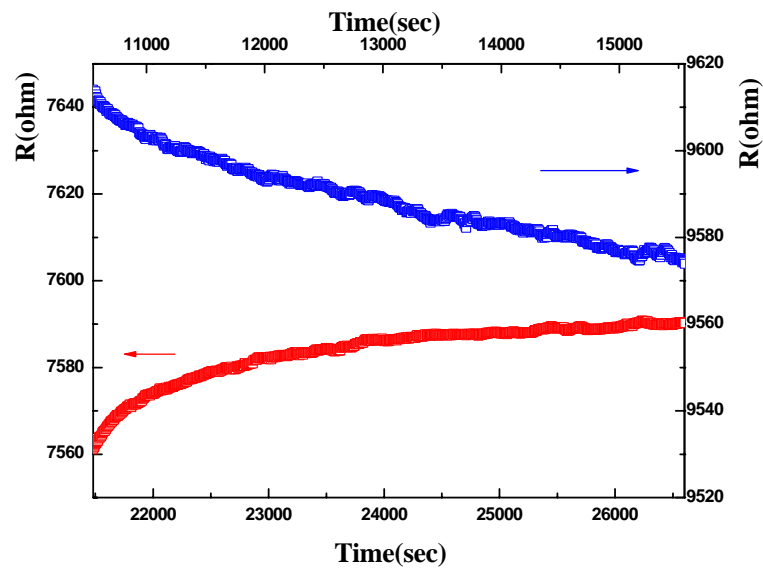
Fig.26 (b) The enlarged diagram illustrates the reversed tendency of resistance

relaxation after removal of H_{th}.
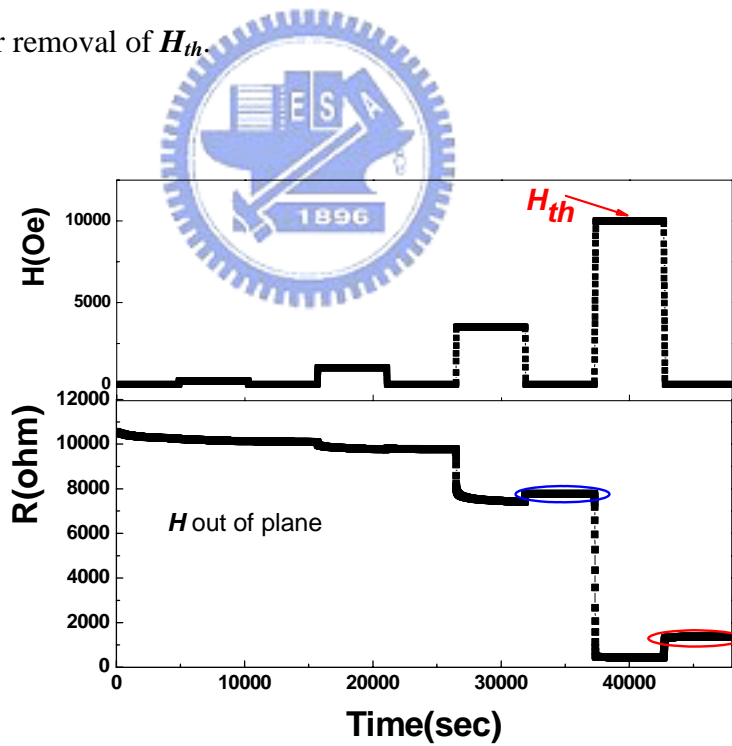
Fig.27 (a) The process of H-out-of-plane experiment with time evolution is illustrated.

We discovered a larger H_{th} as shown.
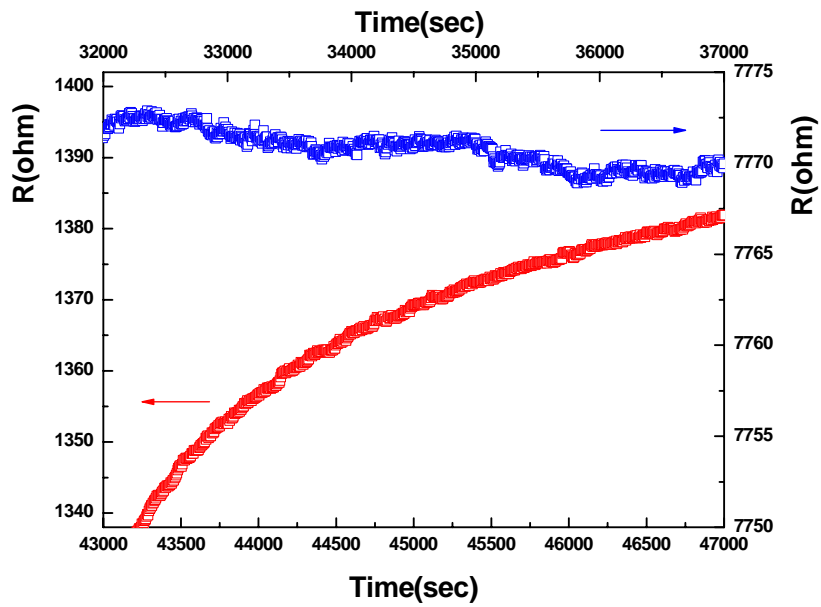
Fig.27 (b) The enlarged diagram illustrates the reversed tendency of resistance

relaxation after removal of H_{th}.
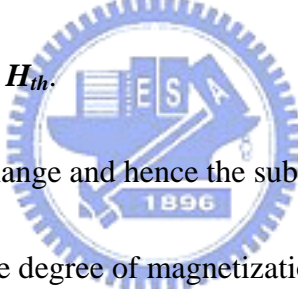
The anisotropy of the change and hence the subsequent relaxation of the resistance is

believed to be related to the degree of magnetization in the sample. Therefore, we've

measured the magnetization-H ($M(H)$) dependence at various temperatures. The results

are summarized in Fig. 28. From diagrams displayed in Fig. 28, especially at low

temperature (e.g. T= 10 K), we can discern the easy axis parallel to H in plane by clear

hysteresis loop. It is reasonable now to infer that the different H_{th} exhibited in the two

applied directions is having the origin of the intrinsic anisotropy of our thin films. In the

remaining of our discussion, we will focus on the results obtained for field applied

in-plane.
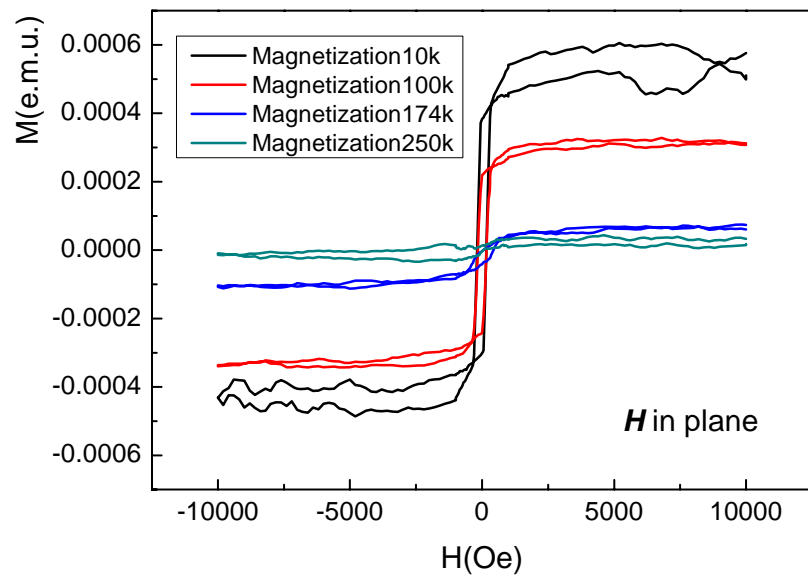
Fig. 28(a) By applying **H** in plane, the hysteresis of **MH** dependence is shown. At

lower temperature, the **M** saturation is larger along with a clearer hysteresis.
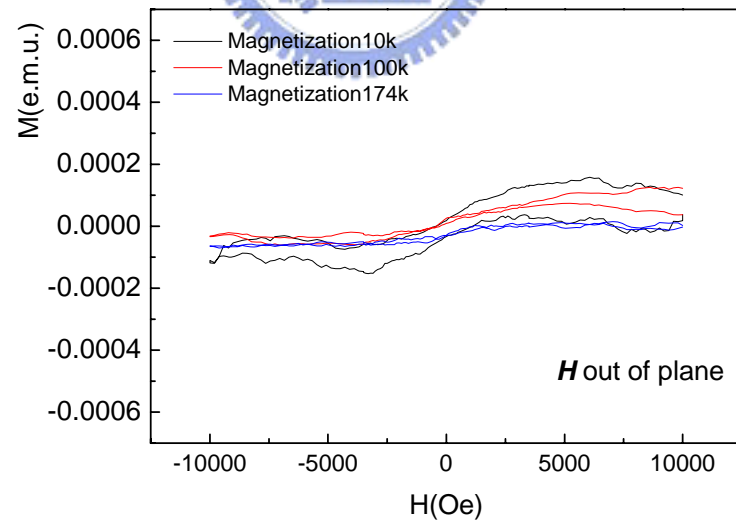
Fig. 28(b) By applying **H** out of plane, we can find no hysteresis behavior within same

magnitude region of **H.** The lack of hysteresis indicates that when **H** is applied out of

plane, it is hard-magnetization-direction for our sample.

(b)The Quenched H_{th} and The "Melting" Magnetic Filed H_m

It is notable that PMME only occurs at certain temperature with a cooling scheme. Upon cooling, the FM phase might not have enough time to reach its equilibrium distribution. Thus, when field H is applied, it may enhance the growth of FM phase and even drive it to exceed the equilibrium proportion. It is under such premise that we can conduct PMME experiment and observe the reverse tendency of resistance relaxation after after removing H. However, if we first cooled LPCMO thin film to low temperature, say T= 10K, the proportion of FM phase at low temperature, though still may not reach its equilibrium proportion, is much larger than that at higher temperatures. Upon warming, due to transformation lagging, FM phase continuously exceeded the equilibrium proportion at certain temperature. In that case, we will not be able to observe the reverse tendency of resistance relaxation, and naturally we cannot define H_{th}—the H_{th} is said to be quenched. The results at different temperatures at which R(T) displays hysteresis namely from T=160 K to T=180 K are shown in Fig.29 (a) (T= 174 K), Fig. 30 (a) (T= 177K), and Fig. 31 (a)(T= 180K, inset shows the enlarged vision).
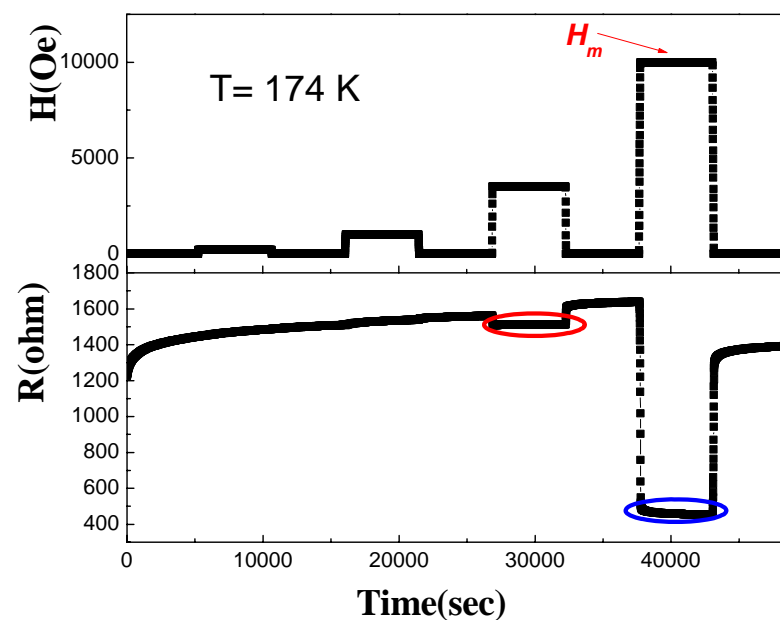
Fig.29 (a) At T = 174 K, as the time evolved, the resistance tended to increase clearly.

The noticeable sudden drop represented a strong MR effect, and the H_m is denoted.
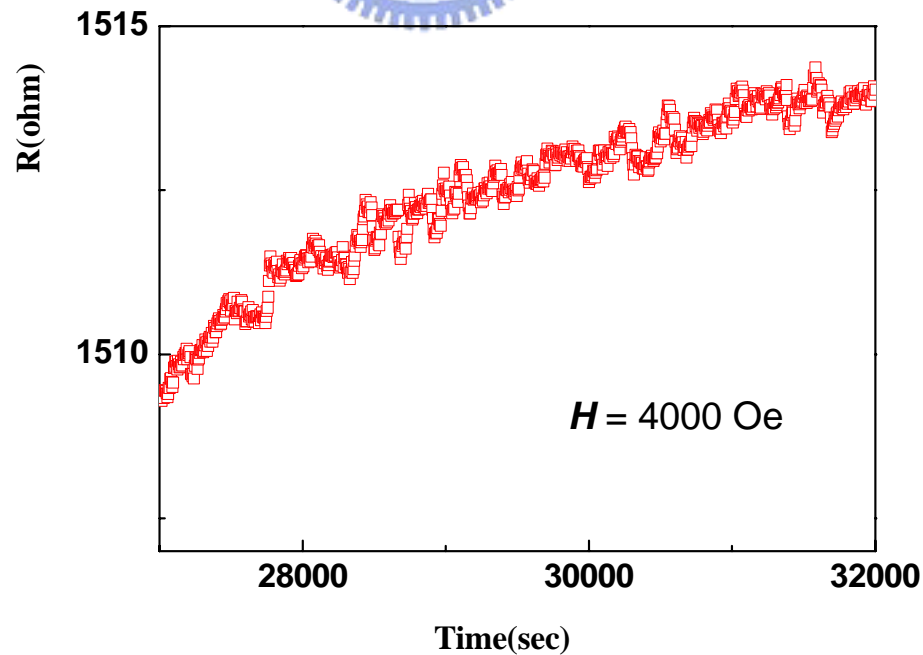

Fig.29 (b) When $H < H_m$, the relaxation tendency still increased.
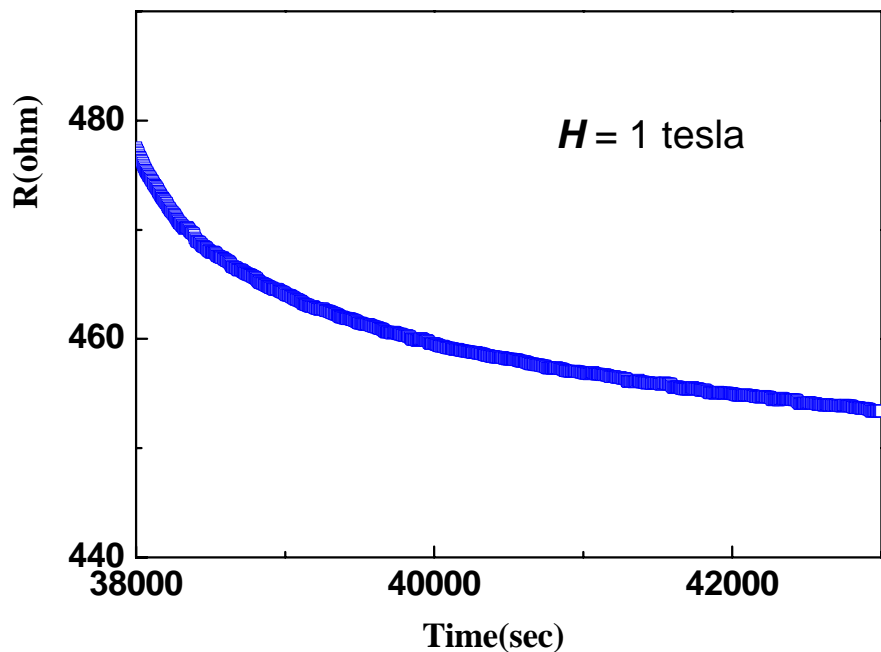
Fig.29 (c) When $H > H_m$, the relaxation tendency decreased.
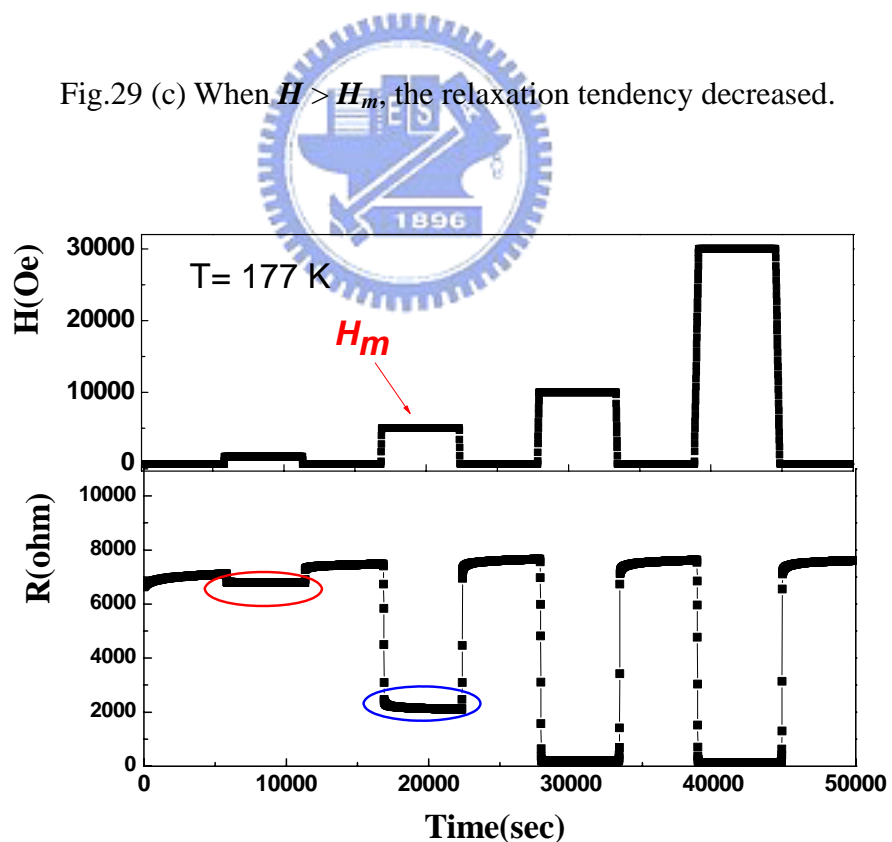
Fig.30 (a) At T= 177 K, the sudden drop occurred with a smaller H_m. Below H_m the

resistance relaxation displays an ascending tendency.
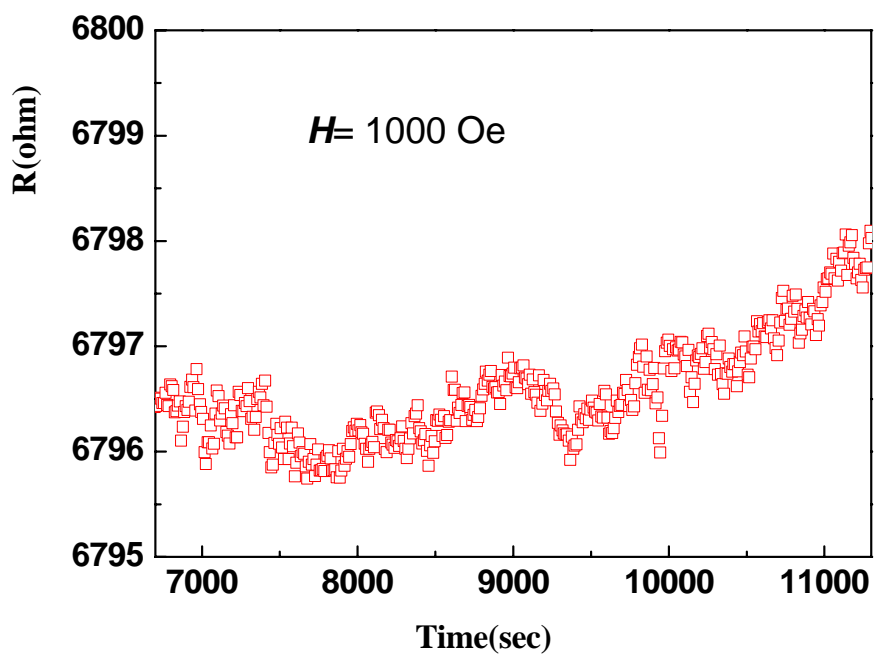
Fig. 30 (b) When $H < H_m$, the relaxation tendency still increased.
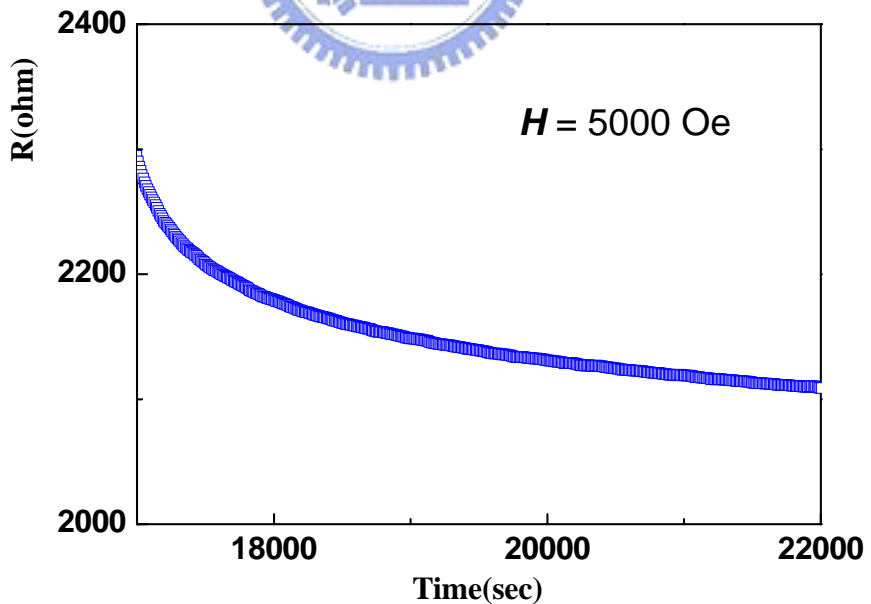
Fig.30 (c) When $H > H_m$, the relaxation tendency decreased.
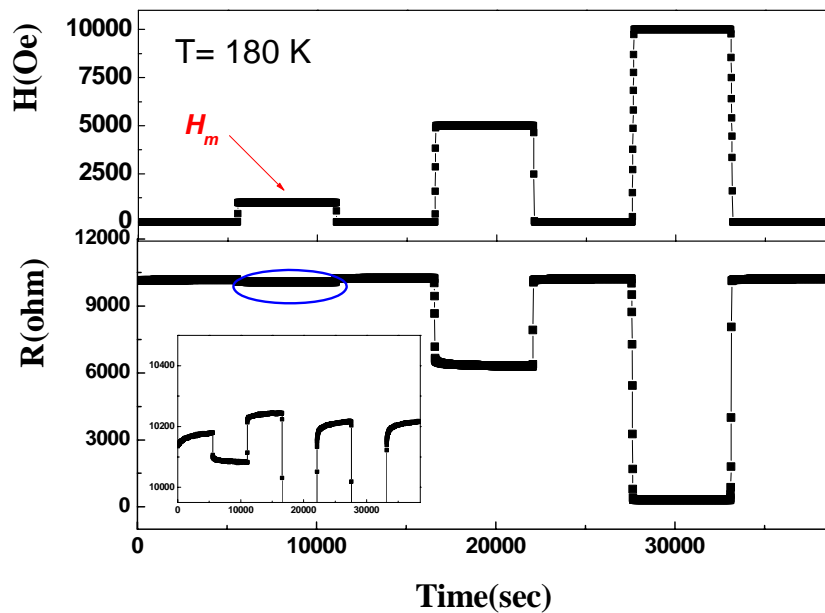
Fig. 31 (a) At T= 180 K, H_m was smaller but without a resistance drop. The inset shows

the enlarged vision of the resistance to scrutinize the relaxation tendency.
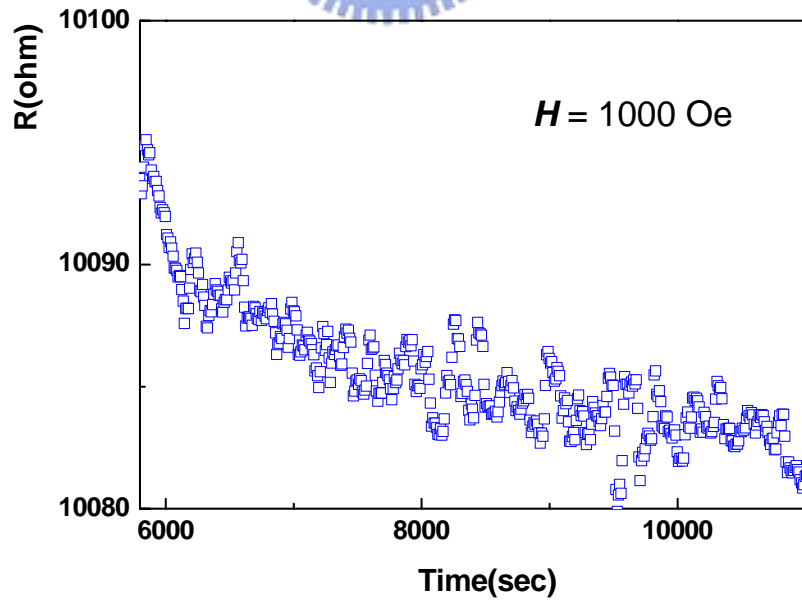
Fig. 31 (b) When $H > H_m$, the relaxation tendency decreases.

Interestingly, at different temperatures, we needed to apply certain magnetic field which is strong enough to "melt" the CO phase. As just mentioned above, the FM phase always exceeded its equilibrium proportion upon the warming scheme. On the other hand, the CO phase continuously grows to reach its equilibrium proportion upon warming protocol. Therefore, we need a strong H, namely H_m, to suppress the growth of CO phase or to "melt" the grown CO phases. This is how we define H_m: we observed the relaxation tendency of resistance while the applied magnetic field was on. With larger and larger H, the tendency changed from ascending to descending. When the tendency just reversed its sign (shown in Fig. 29(c), Fig. 30(c), and Fig.31(b)), the threshold H was defined as H_m.
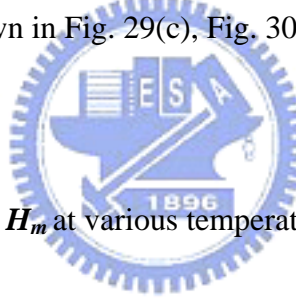
To compare the trend of H_m at various temperatures in this experiment, we tabulated our data in Table 2. Recalling the resistance-temperature dependence shown in Fig. 15, we picked these three temperatures in the hysteresis region: at T= 174 K, the CO phases were still robust and far from its equilibrium proportion, so we needed larger magnetic force (H_m ~1T) to melt the CO phase; at T = 177 K, two phases compete with each other and CO phase is less robust, therefore smaller magnetic field (H_m ~0.5T) is needed to melt CO phase; at T= 180 K, because the CO phase is closer to its equilibrium proportion and is more vulnerable, thus, only a rather small magnetic filed (H_m ~0.1T) is needed to disturb the distribution of CO phase.

	T = 174 K	T = 177 K	T = 180 K
H_m (Oe)	10000	5000	1000

Table 2. The required H_m is smaller with increasing temperature.

b.Time-relaxation Data at Various Temperatures

In this study we tried to attain the metastable resistance-temperature dependence by

utilizing PMME. Nevertheless, at temperature higher than T_{CO} (~200 K), the LPCMO

film should be a single phase state. For this reason, we conducted PMME at T= 250 K

(Fig. 32) and T = 210 K (Fig. 33).
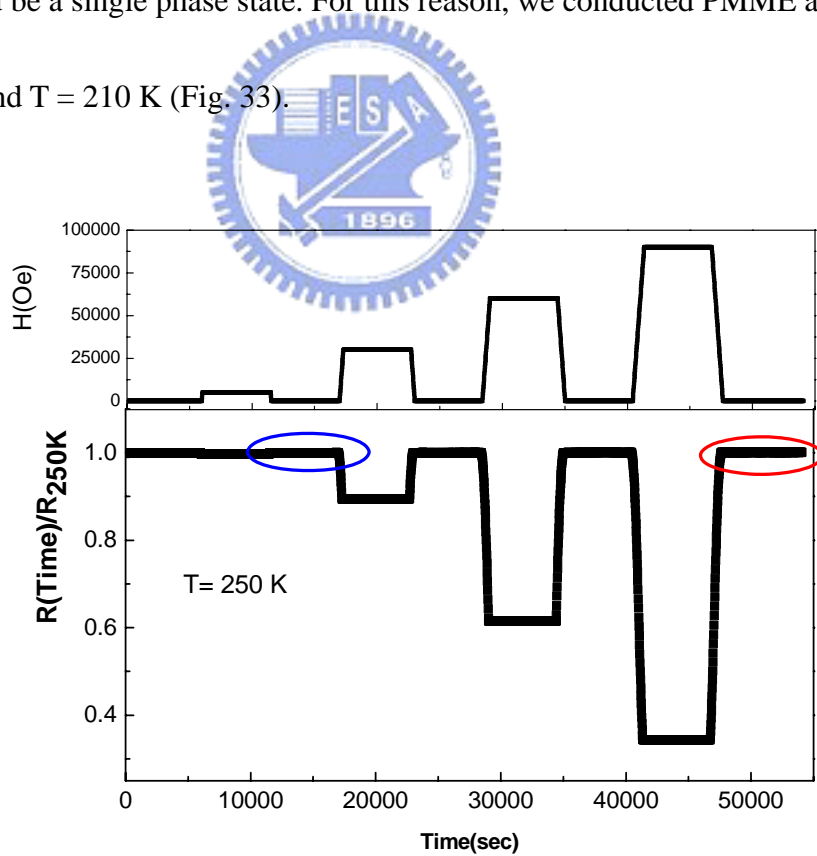
Fig.32 (a) At T = 250 K, even after the largest drop of resistance with H = 9 tesla, the

resistance rejuvenated and kept the same value with time evolving.
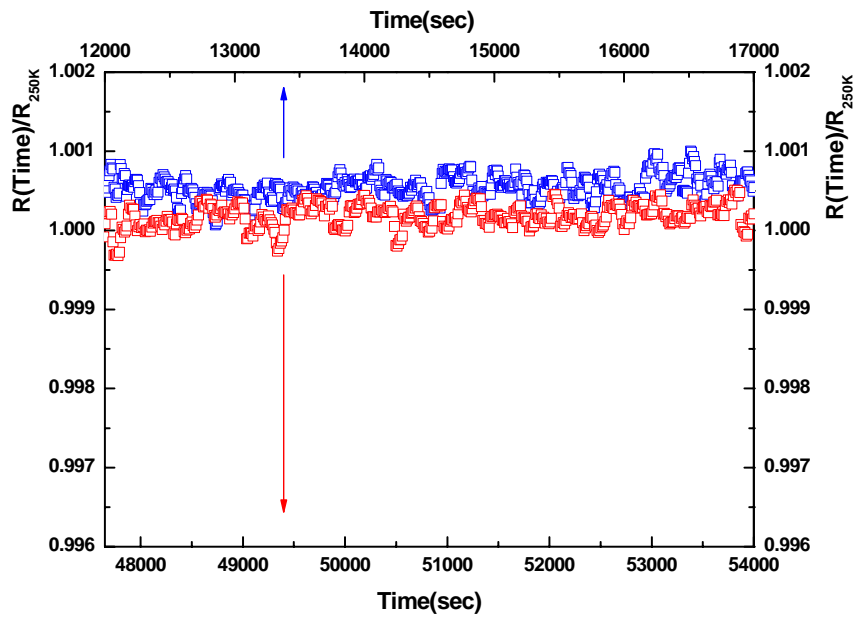
Fig.32 (b) This enlarged diagram reveals the constant value of the resistance before

(blue open circles) and after (red open circles) a large applied **H**.
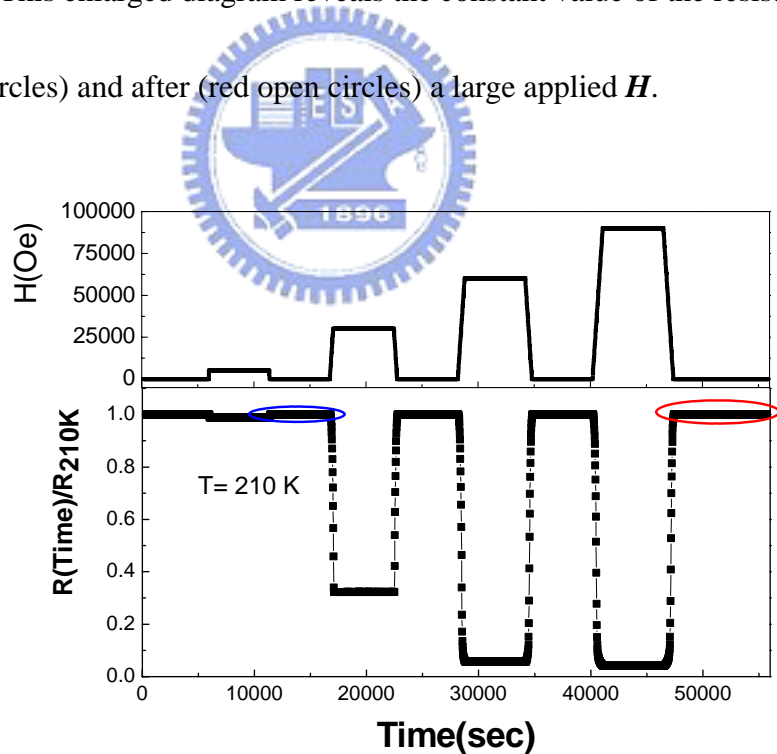
Fig. 33 (a) At T = 210 K, after the largest drop of resistance with **H** = 9 tesla, the

resistance still rejuvenated and kept the same value with time evolving, similar to the

situation at T= 250 K.
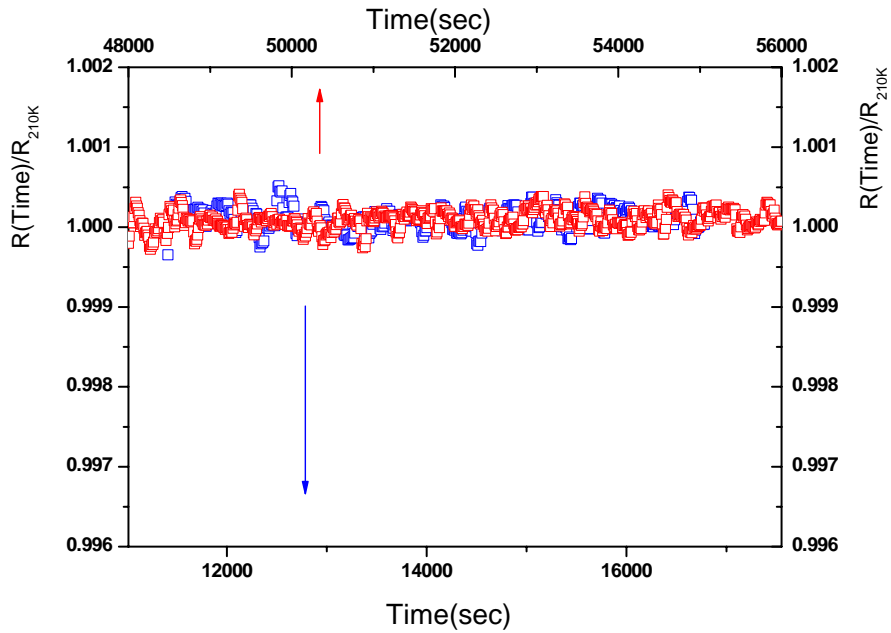
Fig. 33 (b) This enlarged diagram reveals the constant value of the resistance before

(blue open circles) and after (red open circles) a large applied H.

Based on the data displayed in Fig. 32 and Fig. 33, the absence of resistance relaxation

after the removal of the applied field, indicates that the system is in a single phase regime.

In this sense the hysteresis of the electric transport properties described by the PS-model

seems to require that there should be coexistence and competition between the

short-range CO phase and short-range FM phase for observing PMME. In order to

further delineate the point, we carried out PMME experiments over a much wider

temperature range (from 10 K to 190 K) instead of just in the hysteresis region (160 K <

T < 180 K).

Fig. 34 shows the PMME at T= 190 K. Except for a much larger H_{th} (~2T), the

resistance relaxation behaves similarly as previously described. It is suggestive that even at this temperature where noticeable hysteresis is still quite vague the PS has started to emerge. The ratio of the resistance as a function of time (R(T)) and the resistance at T= 190 K was enlarged in fig. 34 (b) to reveal clearer view of relaxation tendency.

Fig. 35, Fig. 36 and Fig. 37 display the PMME in the hysteric region, which is supposed to have the most pronounced effect. As expected, the modulation of resistance was huge and clear with a comparably small H_{th} = **1000 Oe**. The pronounced response to a small perturbation of applied magnetic field, strongly suggest that in the hysterical region, the newly formed CO and FM phases are relative by vulnerable and a small perturbation can affect the competition between the phases.

Fig. 38, Fig.39 and Fig. 40, on the other hand, demonstrate the PMME in the LT region. In this region, generally CO phase and FM phase are both in long-range scale and are both more robust. The magnetic force must be stronger to disturb this metastable state. As we can see in table 3, the H_{th} at T=80 K is 2 tesla while the H_{th} at T= 50 K and T= 10 K is 3 tesla. The magnitude order is same as at T = 190 K and one-order larger than H_{th} in the hysteresis region.

	Above T_{CO}		Below T_{CO}	In the hysteresis region			Low temperature region		
T(K)	250	210	190	177	174	167	80	50	10

$H_{th}(Tesla)$	None	None	2	0.1	0.1	0.1	2	3	3

Table 3. The H_{th} at all temperatures are listed. The H_{max} applied at T= 210 K and T = 250 K was 9 tesla, and we still cannot find the PMME phenomena; therefore we cannot define H_{th} at these two temperatures.
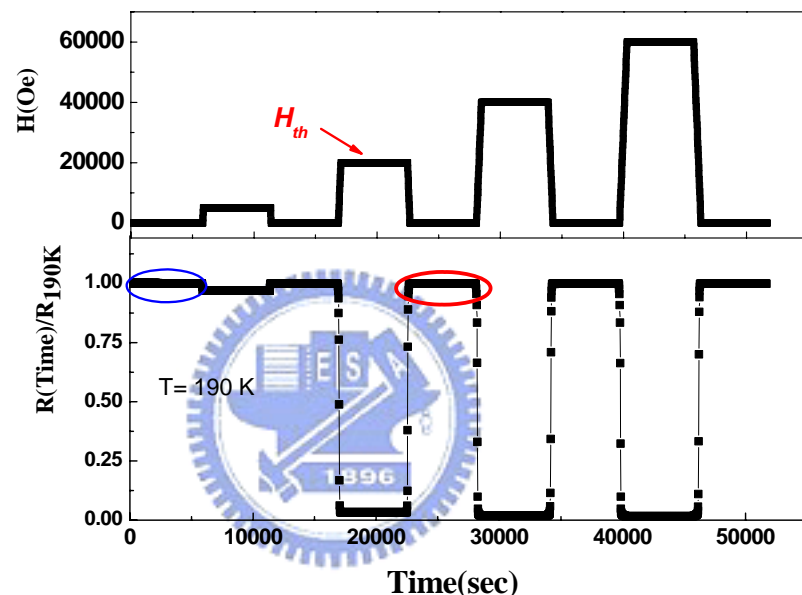

Fig. 34 (a) The PMME experiment at T= 190 K. Notice the sudden drop of resistance accompanied with H_{th}.
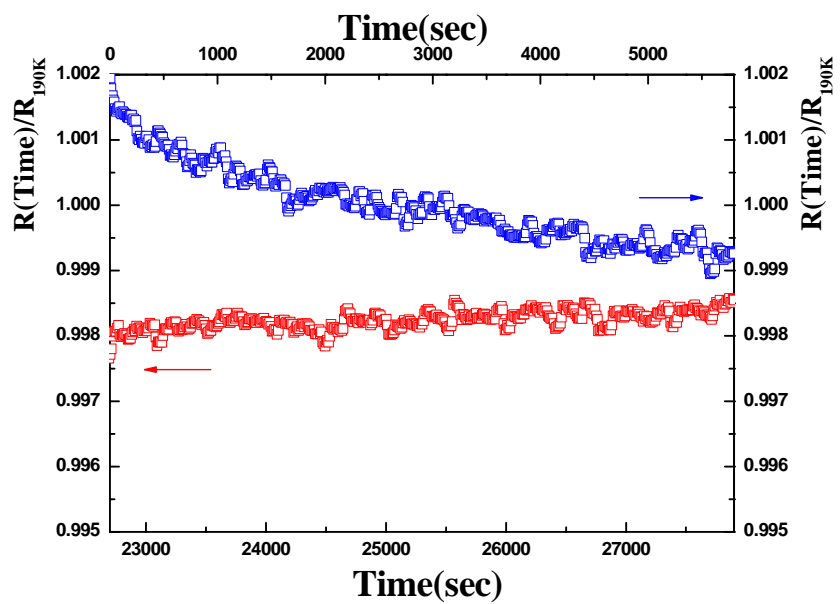
Fig.34 (b) The enlarged plot clarifies the decreasing and increasing relaxation
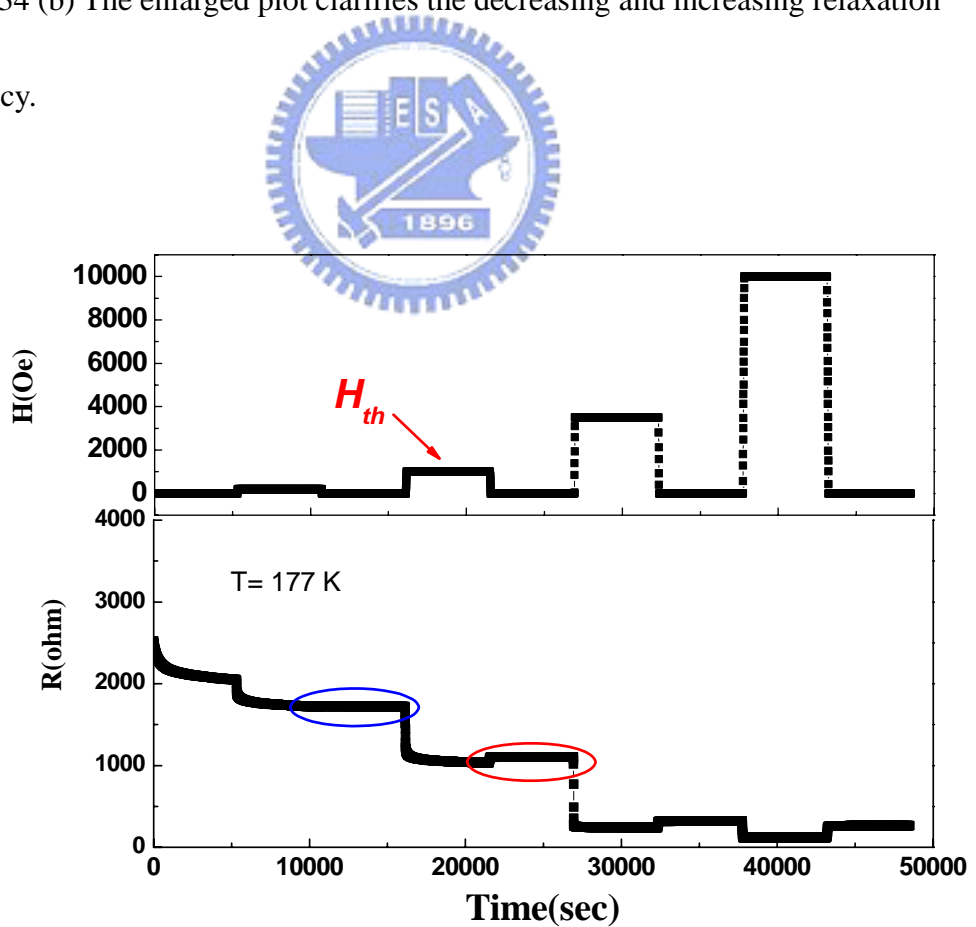
tendency.

Fig. 35 (a) The PMME experiment at T= 177 K.
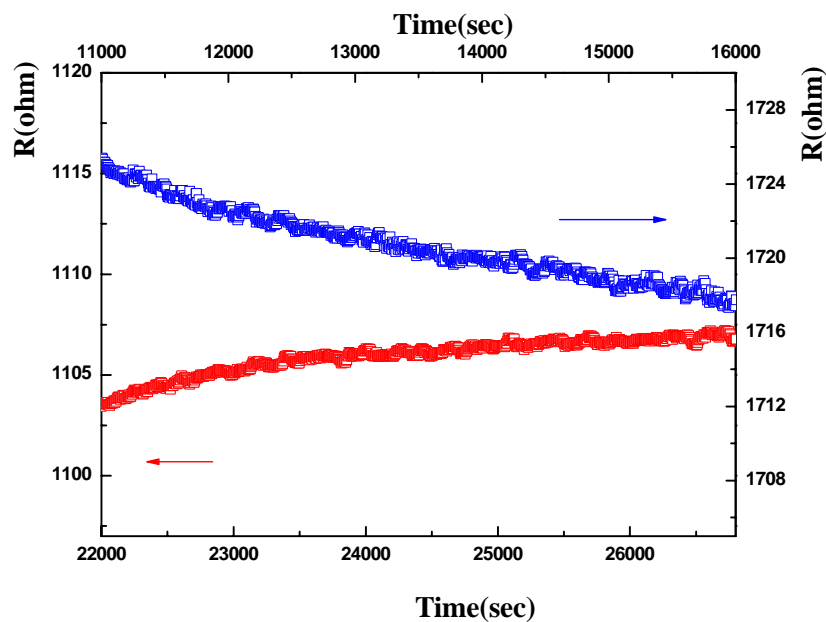
Fig.35 (b) The enlarged plot demonstrates the decreasing and increasing relaxation
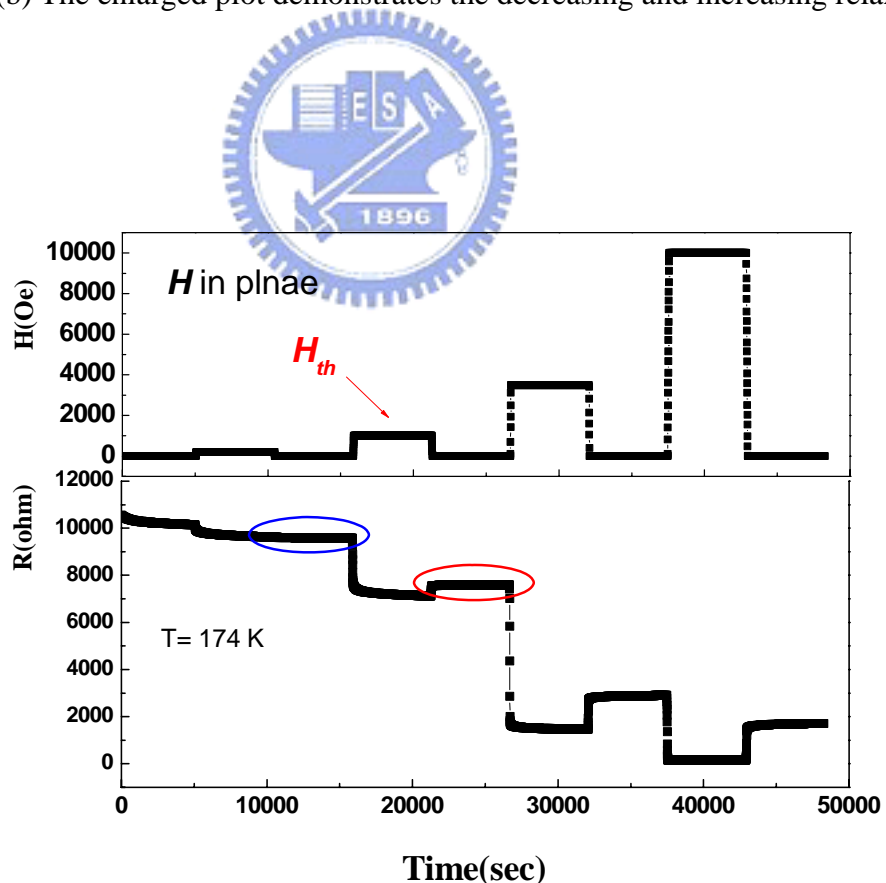
tendency.


Fig.36 (a) The PMME experiment at T= 174 K.
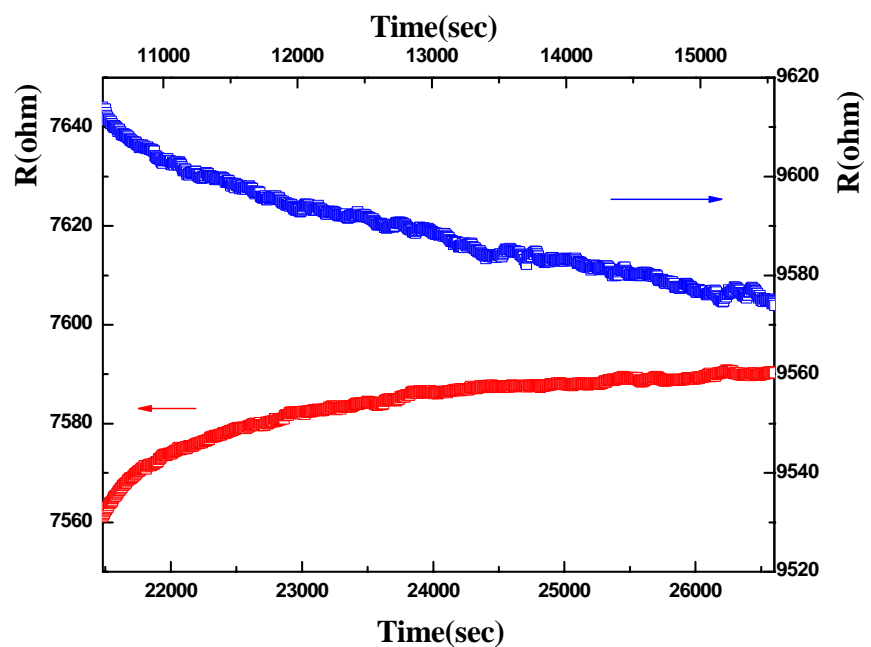
Fig.36 (b) The enlarged plot demonstrates the decreasing and increasing relaxation
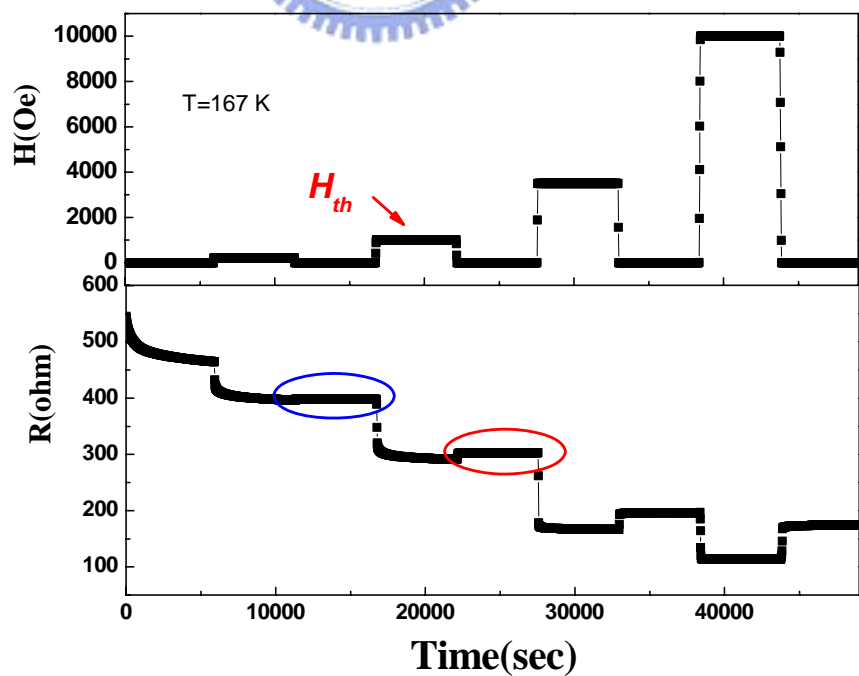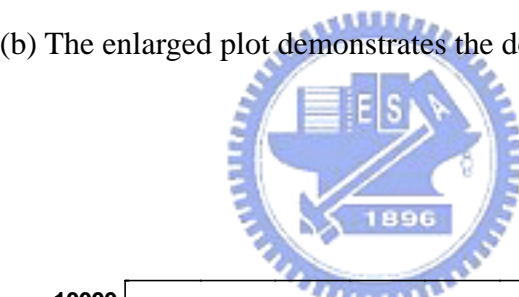
tendency.

Fig.37 (a) The PMME experiment at T= 167 K.
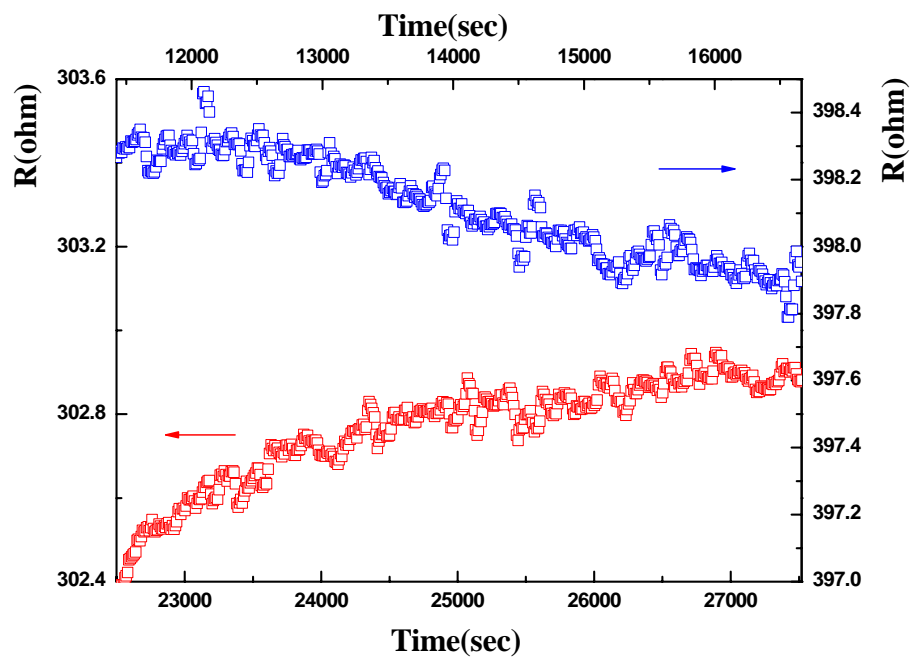
Fig.37 (b) The enlarged plot demonstrates the decreasing and increasing relaxation
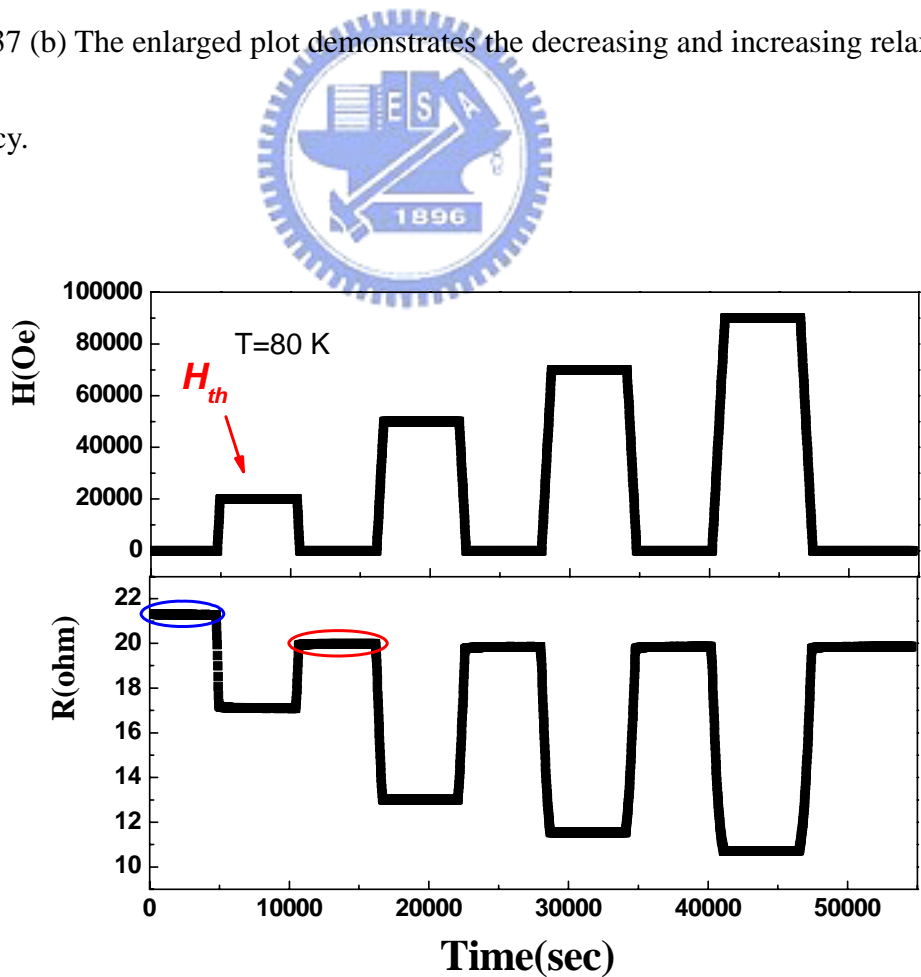
tendency.

Fig.38 (a) The PMME experiment at T= 80 K.
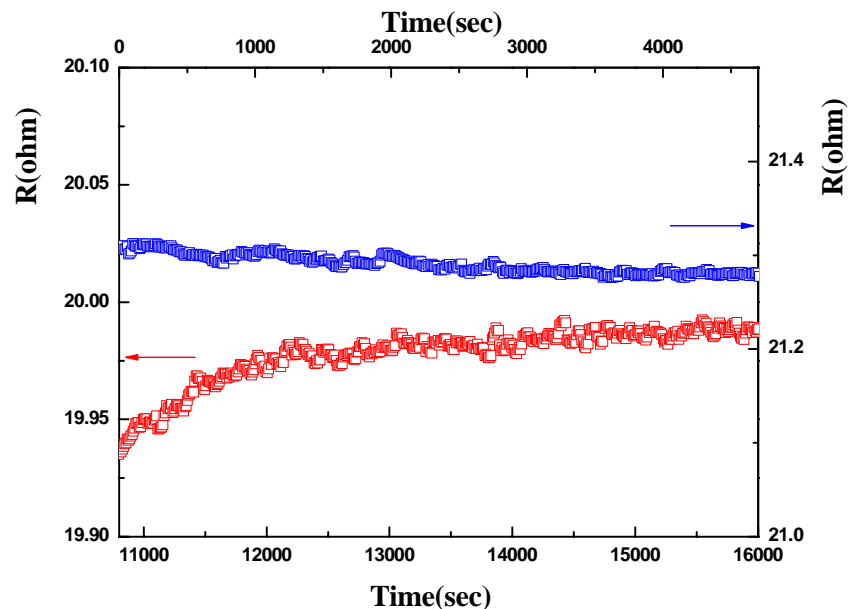
Fig.38 (b) The enlarged plot shows the decreasing and increasing relaxation
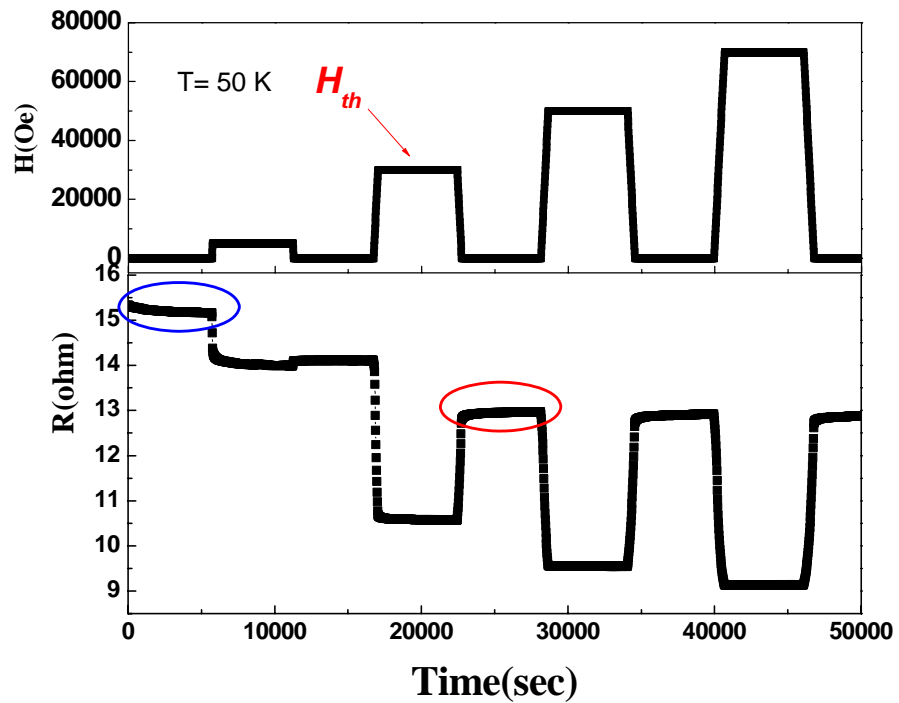
tendency.

Fig.39 (a) The PMME experiment at T= 50 K.
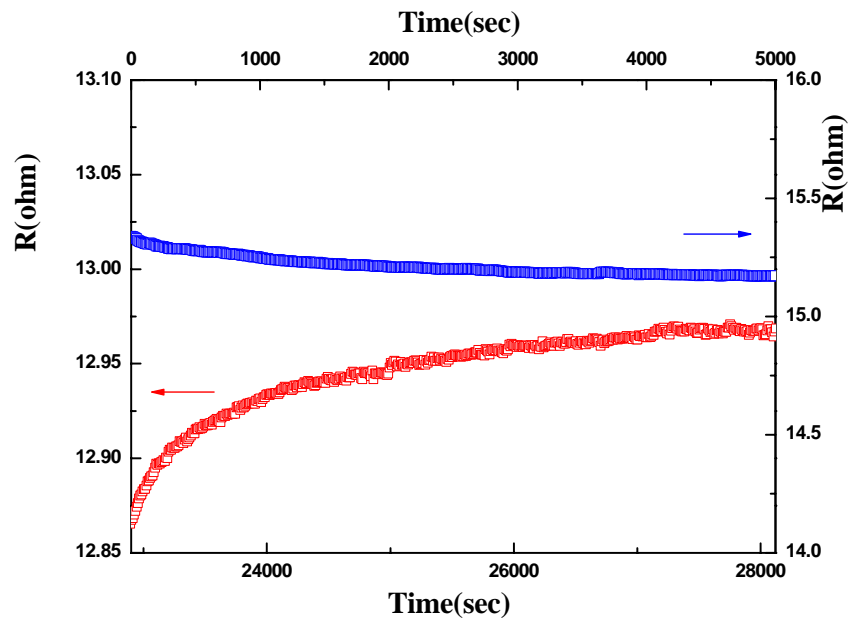
Fig.39 (b) The enlarged plot demonstrates the decreasing and increasing relaxation
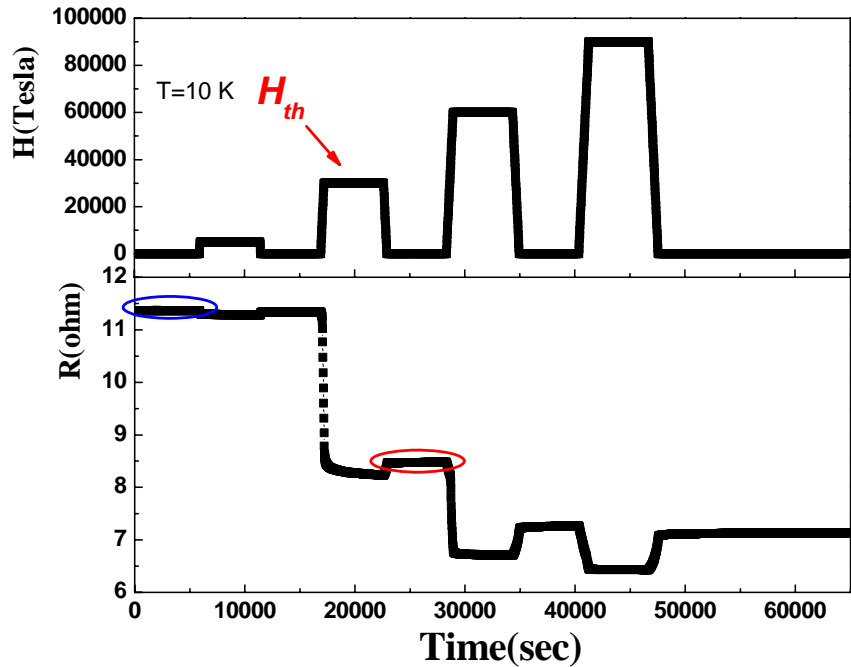
tendency.

Fig.40 (a) The PMME experiment at T= 10 K.
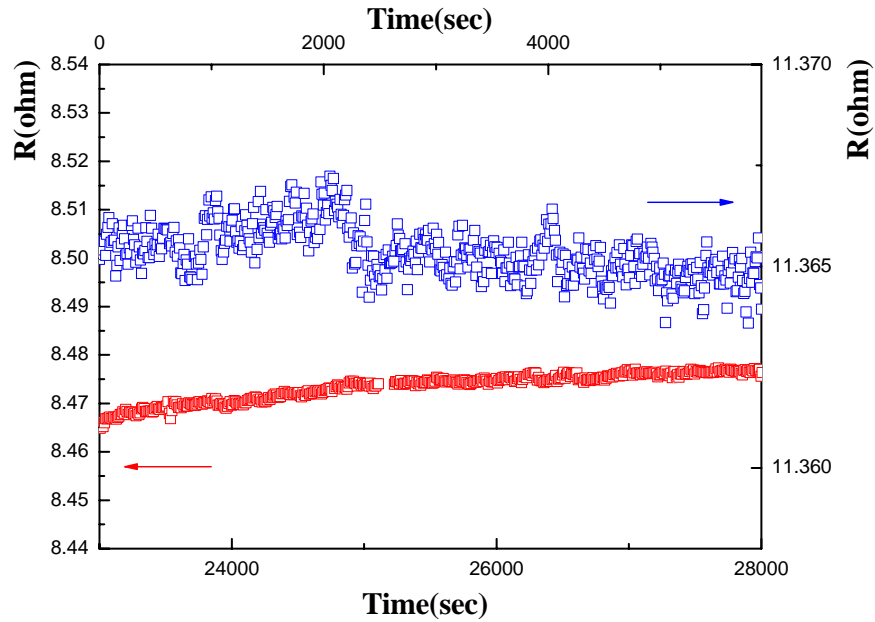
Fig.40 (b) The enlarged plot clarifies the decreasing and increasing relaxation
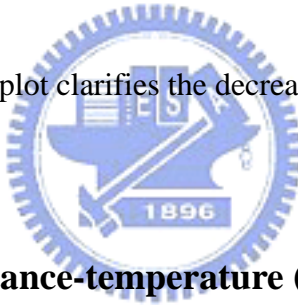
tendency.

c.Metastable Resistance-temperature (RT) dependence

After we conducted the PMME experiments at various temperatures, we could roughly

decide the metastable resistance-temperature (RT) dependence. Fig. 41 illustrates the

metastable RT dependence. Each data plotted in Fig.41 represents a single PMME

experiment at that temperature. Based on the data acquired from the PMME experiments,

we could obtain R_{min}, the minimum resistance from 90-minute relaxation after the

removal of **H** for **H**<**H_{th}**, and R_{max}, the maximum resistance we obtained from 90-minute

relaxation after the removal of **H** for **H**>**H_{th}**. R_{ave} denotes the arithmetic average of R_{max}

and R_{min}. The inset demonstrates, as an example, the difference between R_{max} and R_{min} at

51

T= 190 K. We further compare the obtained metastable RT dependence with that

obtained from a "standard" R(T) measurement (Fig. 42). As is evident from the results,

both values agree quite well, indicating that the current measurements are closely related

to the usual transport measurements.
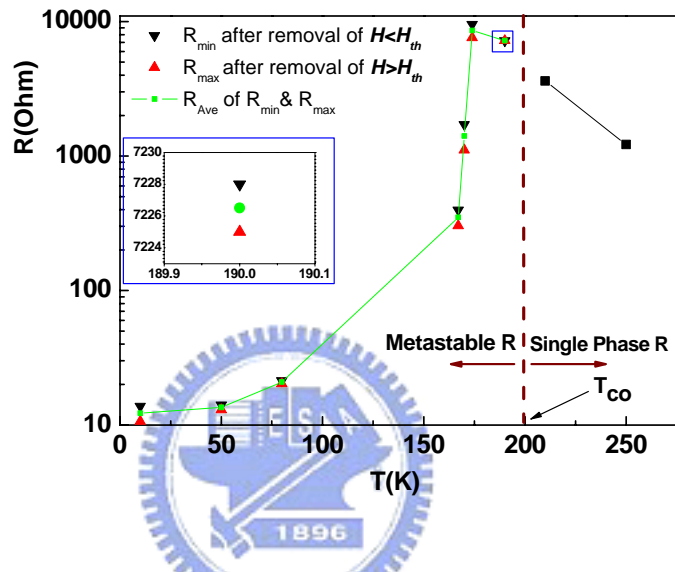
Fig. 41 The diagram shows the single-phase RT dependence above T_{CO} linked with a

black line; a green line indicates the metastable RT dependence.
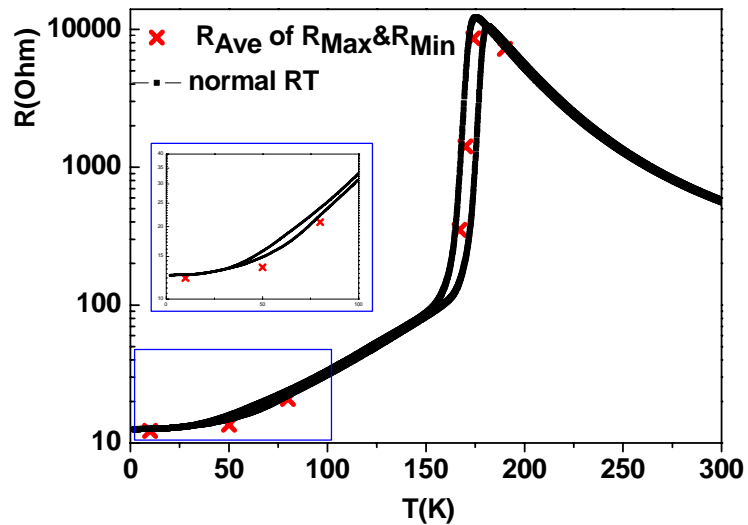
Fig. 42 The plot marks the metastable points of R(T) dependence by red crosses, comparing to that of a standard R(T) measurement. The inset reveals the disability of resistance rejuvenation at low temperatures.

To reconsider the above results obtained form the PMME experiments and the metastable RT dependence we suggest here a possible transport mechanism based on the PS model depicted schematically in Fig.43. This picture is consistent with the model proposed by M. Uehara *et.al* [14], in that emphasis has been focused on the short-range phases. In our case, the short-range phases depicted in Fig.43(a) dominate the transport behavior for temperature just below the T_{CO}; Fig.43(b) illustrates the distribution of the tow separated phases in the hysteresis region. For even lower temperatures the separatede phases become long range ordered phases and as depicted schematically in Fig.43(c). As our PMME results revealed at T= 190 K, the applied *H* did not affect the transport behavior very much because of the size and amount of the two phases and still too tiny to dominate the transport properties. On the other hand, PMME data in the hysteresis region indicated that a strong disturbance in resistance could be made with a small applied *H,* suggesting that not only the size and amount of the two phases become large enough to determine the transport properties but also they are susceptible to relatively lower field. Finally, for lower temperatures, an even larger *H* is needed for observing PMME. This can be understood since at these

temperatures the two separated phases are in long-range order regime and may become

robust enough and are difficult to be disturbed by external fields.
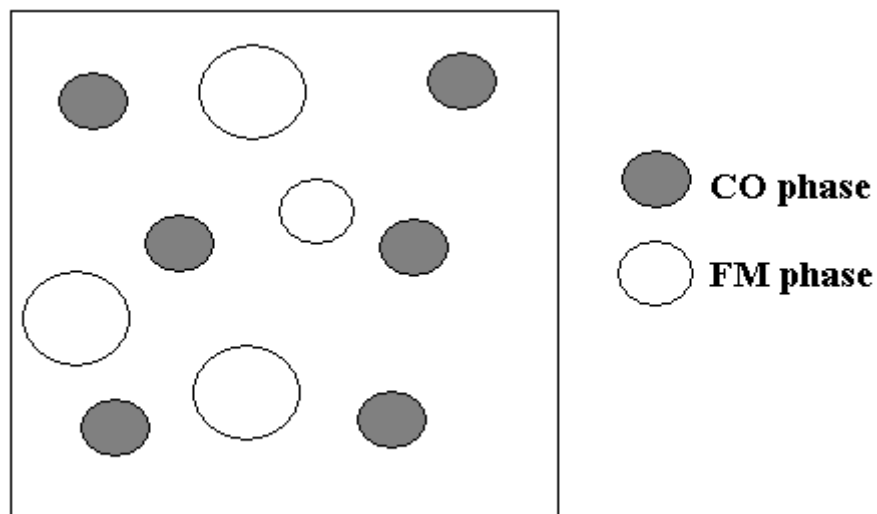

Fig. 43 (a) Illustration of the two separated phases at temperature just below T_{CO} to

indicate the CO and FM phases just start to grow and the sizes are small.
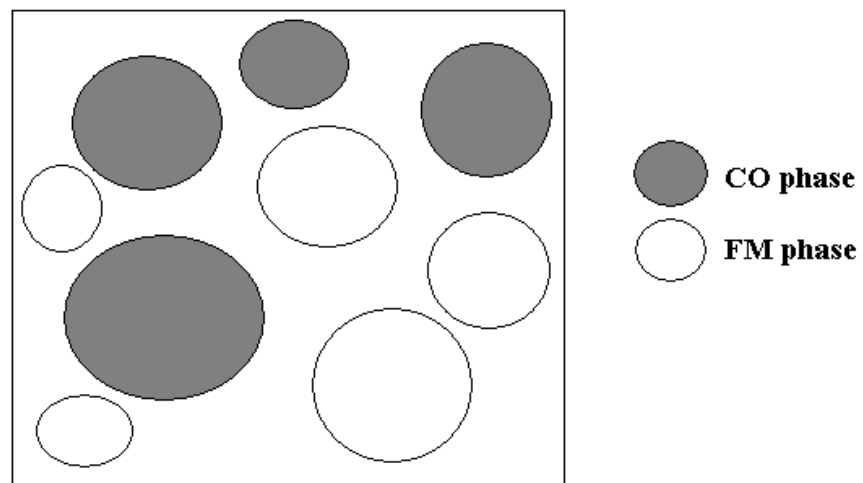
Fig.43 (b) Illustration of the two separated phases in the hysteresis region where the

CO phases and FM phases are larger and compete with each other intensively.
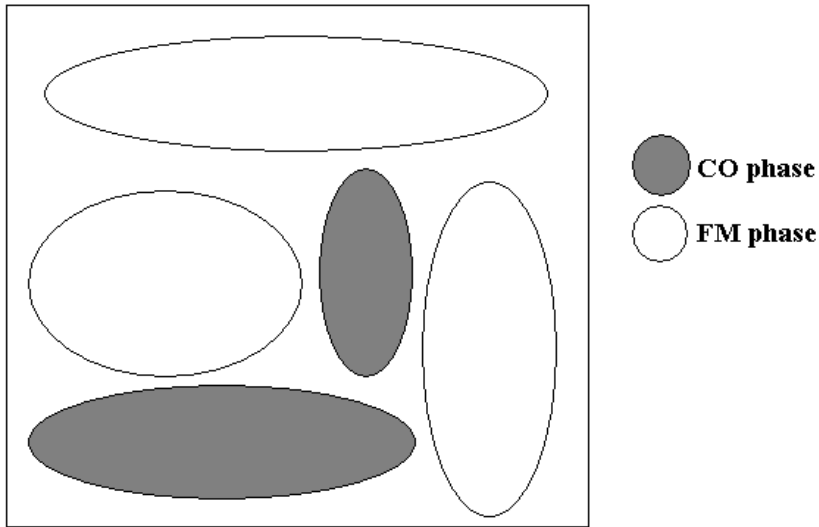
Fig.43 (c) Illustration of the two separated phases at low temperature suggests the

long-range CO and FM phases' existence and the disturbance affect less in this region.

d.R-H Oscillation Experiments at Various Temperatures

To further depict the scenario proposed above, we conducted R-H oscillation

experiments at T=190 K (Fig.44, just below T_{CO}), T= 174 K (Fig.45, in the hysteresis region),

and T= 130 K (Fig.46, at low temperature). These experiments were designed to use the

oscillating field to "stir" the metastable state that will effectively remove the effect of H_{th} and

hence accelerate the relaxation. We first cooled the sample to the temperature aimed. Then,

we applied a H which is larger than H_{th}, removed it, and measured the resistance relaxation

for 200 minutes. This is done in order to compare subsequently the behaviors under

oscillating H the same period of time. Finally, we applied an descendent oscillating H and

measured the change of the resistance simultaneously over the same period of time. The

results measured at T= 190 K is shown in Fig. 44(a). In this case, both the zero-field

relaxation and oscillating field "stirred" relaxation display consistent behaviors with an

increasing relaxation in R. Fig. 44(b) illustrates the R-H hysteresis loops upon the R-H

oscillation. The fact that the size of each loop responding to the descending field remains

essentially the same is indicative of a relatively undisturbed phase-separation distribution

under such conditions. Since H_{th} (190 K) ~ 2 T I smuch larger over than the $H_{osc.}$(max)

applied here, we expect that the $H_{osc.}$ applied here, though effectively changed the overall

resistance by maybe usual magnetoresistance behavior, does not alter the phase separation

distribution and hence did not affect the resistance relaxation (or PMME). Fig. 45(a) shows

the results at T= 174 K, revealing that the stirring of the applied oscillating field causes an

even larger increase in resistance with time than the original zero-field relaxation over the

same duration of time. Fig. 45(b) shows a distinctly different R(H) hysteresis at this regime.

The larger hysteresis R(H) loops indicates even a small field can affect the transport behavior

significantly. We believe that in this temperature regime, since the coexisting new phases start

to play a more significant role in determing the transport properties and are not yet robust

enough. Thus, the resistnace is susceptible to even a small field. However, at T = 130 K (as

shown in Fig. 46(a) and 46(b)) even the applied field is as large as 3 Tesla, due to the

robustness of the long range ordered CO and FM phases, only very little hysteretic effects are

discernible.
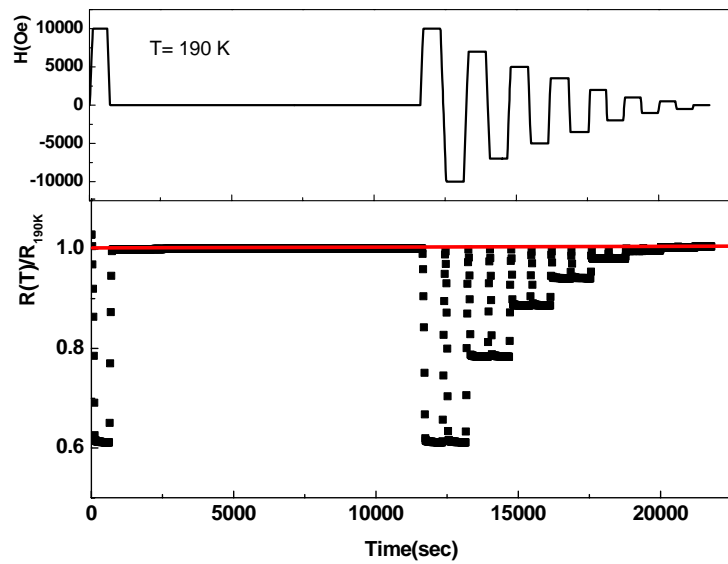
Fig.44(a) The red line represents the original increasing relaxation tendency. After the

R-H oscillation, the resistance relaxation still follows the original tendency.
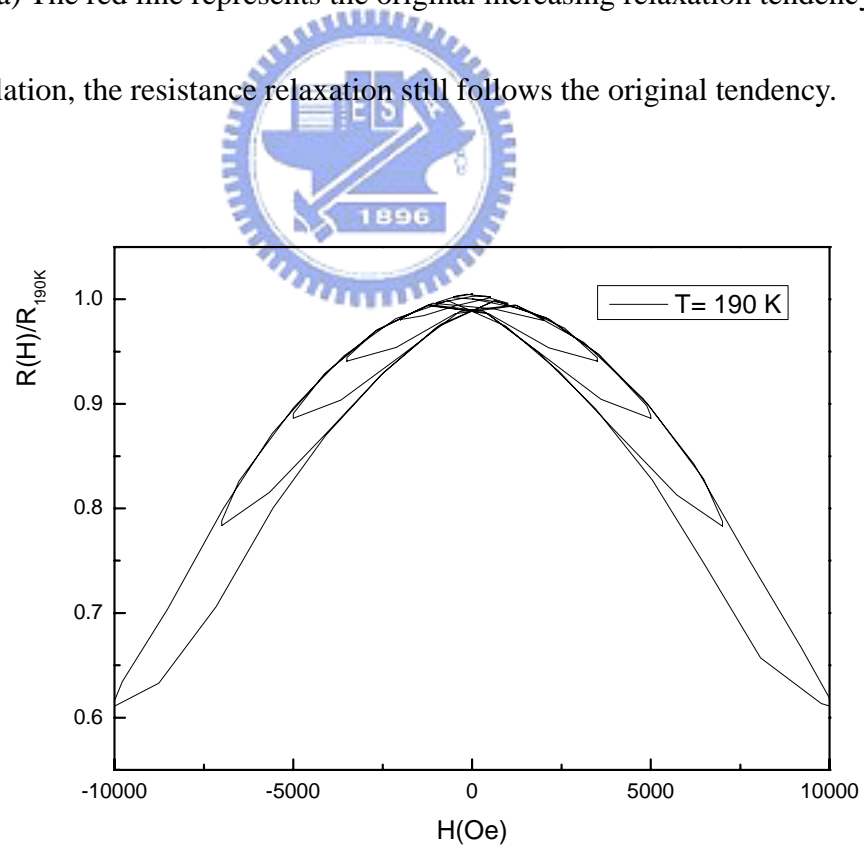

Fig.44(b) The symmetric hysteresis of R-H with *H* oscillation is clearly observed.
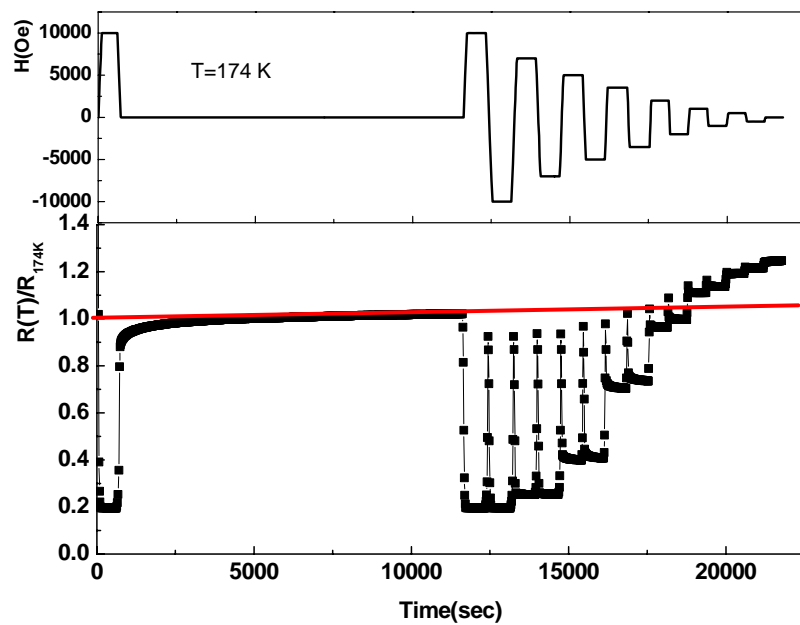
Fig.45(a) The red line represents the original increasing relaxation tendency. After the

R-H oscillation, the resistance relaxation tendency increased more than the original.
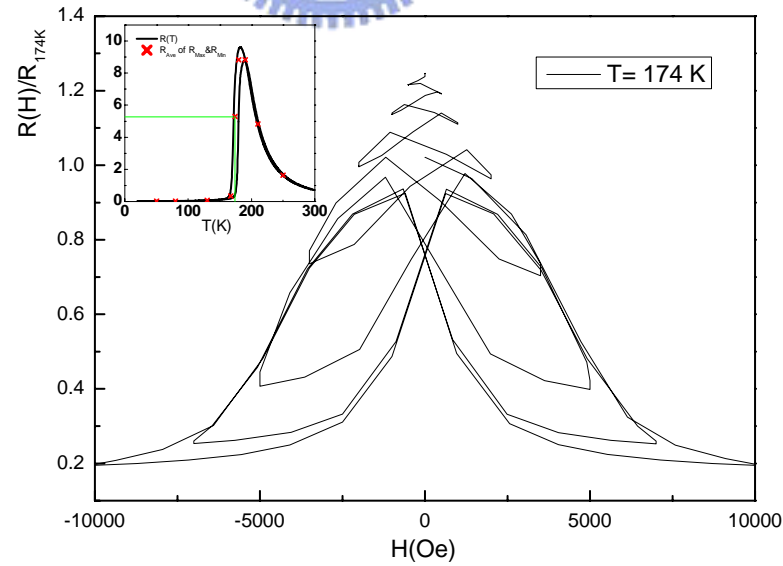
Fig.45(b) The symmetric R-H hysteresis is clearer and larger with same *H* oscillation

than that at T= 190 K.
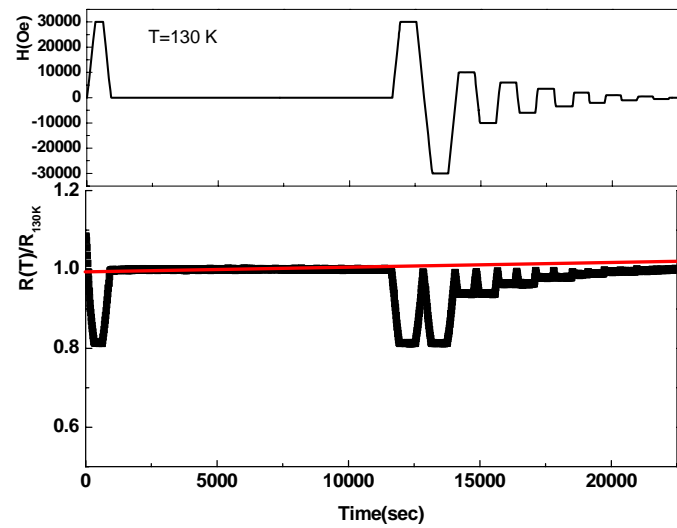
Fig.46(a) Fig.41(a) The red line represents the original increasing relaxation tendency.

After the R-H oscillation, the resistance relaxation shows a slight decrease, comparing to

the original tendency.
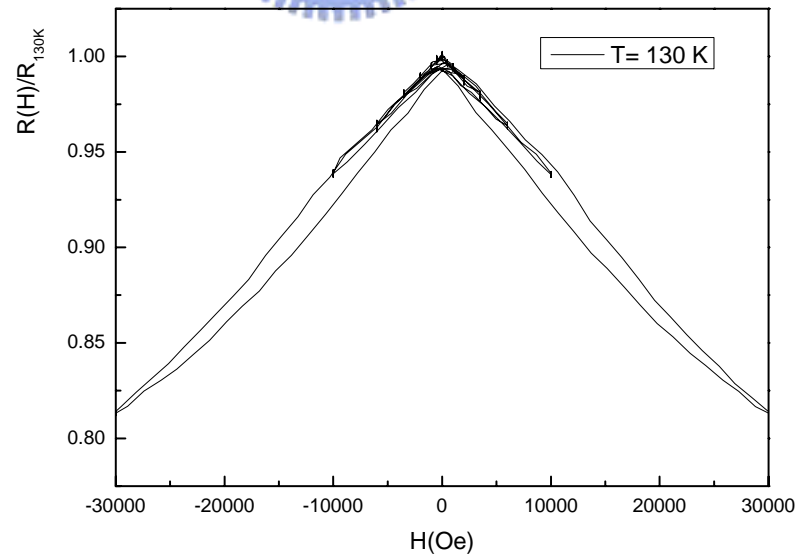
Fig.46(b) The R-H hysteresis is small even with a larger *H* oscillation at T= 130 K.

Chap.5 Summary and Conclusions

In discussing the nature and consequences of the phase separation model, we propose

a size-effective mechanism to relate the detailed distribution of the coexisting phases to

the measured magneto-transport properties. By studying the time-relaxation of resistance

at different temperatures, properties have been shown to intimately correlate the electric

transport with competitions between the coexisting phases. In particular, we

demonstrated that, although the PMME phenomena can be discerned over a much wider

temperature range than previously anticipated, the properties are most susceptible to

external disturbances (e.g. temperature change or applied magnetic field) when it is in

the vicinity of phase transition regime. Our experiments also demonstrated that both the

amount and robustness of the CO phases may be playing the dominant role in giving rise

to the R (T) hysteresis in LPCMO. This may also explain why the PMME is absent in

LCMO system. Fig. 47 illustrates the different phase transitions with decreasing

temperature in the two systems. The hysteretic and the relevant relaxation behaviors

observed in this study could be due to two possibilities resulted from the formation of

CO phase. One is the existence of CO-phase is the sole reason. The other is that the

behavior may be general for phase coexistent systems; nevertheless, the relaxation

process is too fast for the FM phase as compared to that of the CO phase. Thus, we only

see the manifestations of the CO phase. Further work is certainly needed to discern these

proposed possibilities.
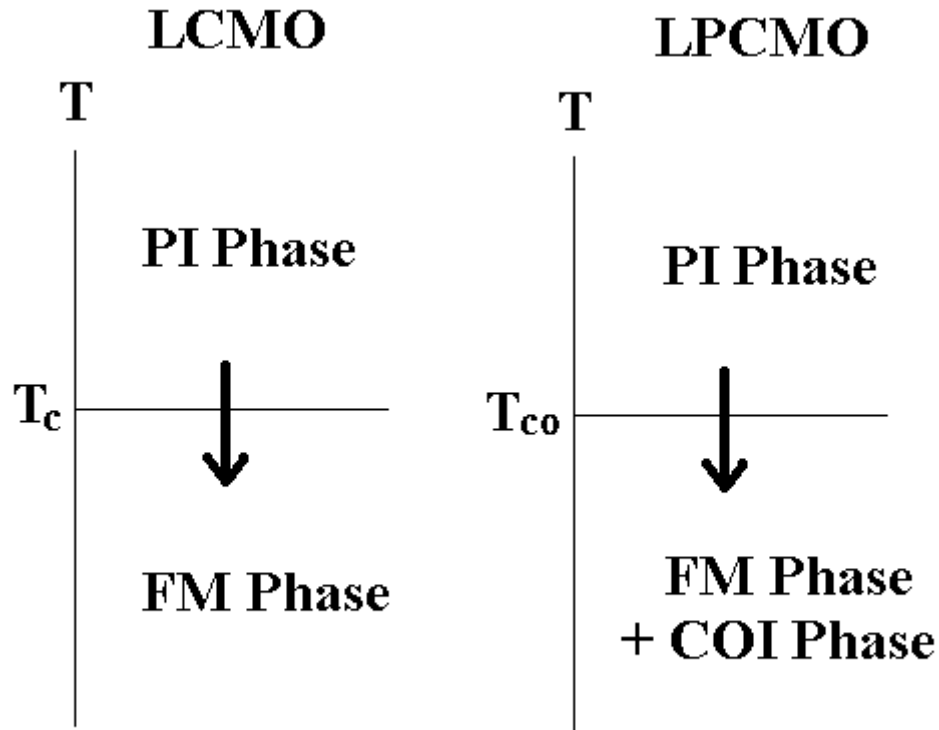
Fig. 47 A schematic illustration expresses the phase transition with decreasing

temperature in LCMO and LPCMO. **PI** denotes the paramagnetic insulator, **FM** denotes

the ferromagnetic metal, and **COI** denotes the charge-ordering insulator.

References

[1]G.H. Jonker and J.H. van Santen, Physica **16**, 337 (1950).

[2] G. C. Xiong, Q. Li, H. L. Ju, S. M. Bhagat, S. E. Lofland, R. L. Greene, and T. Venkatesan, Appl. Phys. Lett. **67**, 3031 (1995).

[3]C.Zener, Phys. Rev. 82, 403 (1951).

[4]H.Y. Hwang , S-W Chenog, P.G. Radaelli, M.Marezio, and B.Batlogg, Phys. Rev. Lett. **75**, 914 (1995).

[5]N. Mannella, A.Rosenhahn, C.H. Booth, S. Marchesini, B.S. Mun, S.-H. Yang, K. Ibrahim, Y. Tomioka, and C.S. Fadley, Phys. Rev. Lett. **92**, 166401(2004).

[6]M. Jaime, M.B. Salamon, M. Rubinstein, R.E. Treece, J.S. Horwitz, and D.B. Chrisey, Phys. Rev. B **54**, 11914(1996).

[7] O. Toulemonde, F. Studer, A. Barnabé, A. Maignan, C. Martin, B. Raveau**,** J. Phys. **11**,109(1999).

[8]Jan Burgy, Adriana Moreo, and Elbio Dagotto, Phys. Rev. Lett. **92**, 097202(2004).

[9]F. Parisi, P.Levy, L.Ghivelder, G.Polla, and D. Vega, Phys. Rev. B **63**,144419(2001).

[10J.X. Ma, D.T. Gillaspie, E.W. Plummer, and J. Shen, Phys. Rev. Lett. **95**, 237210(2005).

[11]A.Masuno, T.Terashima, Y.Shimakawa, and M. Takano, Appl. Phys. Lett. **85**, 6194(2004).

[12] E.S. Vlakhov, K.A. Nenkov, T.I. Donchev, E.S. Mateev, R.A. Chakalov, A.Szewczyk, M.Baran, and K.Piotrowski, J. Mag. Mag. Mate. **290**,955(2005).

[13]A. Moreo, Seiji Yunoki, and Elbio Dagotto, Science **283**, 2034(1999).

[14]M.Uehara, S.Mori, C.H. Chen and S.-W. Cheong, Nature **399**, 560(1999).

[15]Liuwan Zhang, Casey Israel, Amlan Biswas, R.L.Greene, and Alex de Lozanne, Science **298**, 805(2002).

[16]L. Ghivelder and F.Parisi, Phys. Rev. B **71**, 184425(2005).

[17]M.tokunaga, Y.Tokunaga, and T.Tanegai, Phys. Rev. Lett. **93**, 037203(2004).

[18]N.A. Babushkina, L.M. Belova, D.I. Khomskii, K.I.Kugel, O.Yu. Gorbenko, and A.R. Kaul, Phys. Rev. B **59**, 6994(1999).

[19]S. Taran, Sandip Chatterjee, and B.K. Chaudhuri, Phys. Rev. B **69**, 184413(2004).

[20]A. S. Ogale, S.R.Shinde, V.N. Kulkarni, J.Higgins, R.J. Choudhary, Darshan C. Kundaliya, T.Polleto, and S.B.Ogale, Phys. Rev. B **69**, 235101(2004).

[21]M. Quintero, A.G.Leyva, P.Levy, F.Parisi, O.Aguero, I.Torriani, M.G. das Virgens, L.Ghivelder, Physica B **354**, 63(2004).

[22]T. Wu, S.B. Ogale, S.R.Shinde, Amlan Biswas, T.Polletto, R.L.Greene, and A.J. Millis, J. Appl. Phys. **93**, 5507(2003).

[23]P. Levy, F. Parisi, L. Granja, E. Indelicato, and G.Polla, Phys. Rev. Lett. **89**, 137001(2002).

[24]V. Markovich, E.S. Vlakhov, Y.Yuzhelevskii, B. Blagoev, K. A. Nenkov, and

G.Gorodetsky, Phys. Rev. B **72**, 134414(2005).

[25] P. Levy, F. Parisi, M. Quintero, L. Granja, J. Curiale, J. Sacanell, G. Leyva, and G. Polla,

Phys. Rev. B **65**, 140401(2002).

[26]D.D.Sarma, Dinesh Topwal, U.Manju, S.R. Krishnakumar, M.Bertolo, S.La Rosa,

G.Cautero, T.Y. Koo, P.A. Sharma, S.-W. Cheong, and A. Fujimori, Phys. Rev. Lett. **93**,

097202(2004).

[27]A. J. Millis, P. B. Littlewood, and B. I. Shraiman, Phys. Rev. Lett. **74**, 5144(1995).

[28]J.M. De Teresa, M.R. Ibarra, P.A. Algarabel, C.Ritter, C.Marquina, J.Blasco, J.Garcia,

A.del Moral, and Z.Arnold, Nature **386**, 256(1997).

[29]Y.Tokura and N. Nagaosa, Science **288**, 462(2000)

[30]simple interpretation could be found in *Introduction to Solid State Physics*, C. Kittel, 1953

[31]T. Tomioka and Y. Tokura, Phys. Rev. B **70**, 014432(2004).

[32]S. Dong, Han Zhu, X.Wu, and J.-M. Liu, Appl. Phys. Lett. **86**, 022501(2005).

[33]E. Dagotto, Science **309**, 257(2005).

[34]STM image provided by W.J. Chang, department of electrophysics, National Chiao Tung

University, Taiwan

[35] These figures are illustrated by Matthias Mayi

[39]J.Y. Lin, C.W. Chen, Y.C. Liu, S.J. Liu, K.H. Wu, Y.S. Gou, and J.M. Chen, J. Mag. Mag

Mate. **239**, 48(2002).

[40]F.M.F. de Groot, M. Grioni, J.C. Fuggle, J.Ghijsen and G.A. Sawatzky, and H. Petersen,

Phys. Rev. B **40**, 5715(1989).

[41]H.L. Ju, H.-C.Sohn, and Kannan M. Krishnan, Phys. Rev. Lett. **79**, 3230(1997).

[42]G.M. Zhao, V.Smolyaninova, W. Prellier, and H.Keller, Phys. Rev. Lett. **84**, 6086(2000).

[43]H. Eskes, M.B.J. Meinders, and G.A. Sawatzky, Phys. Rev. Lett. **67**, 1035(1991).

[44]J.H. Park, C.T. Chen, S-W. Cheong, W.Bao, G.Meigs, V.Chakarian, and Y.U. Idzerda,

Phys. Rev. Lett. **76**, 4215(1996).

[45]J.H. Park, T.Kimura, and Y. Tokura, Phys. Rev. B **58**, 13330(1998).